

Gradient Approximation and Multivariable Derivative-Free Optimization Based on Noncommutative Maps

Jan Feiling D, Mohamed-Ali Belabbas D, and Christian Ebenbauer D, Member, IEEE

Abstract—In this article, multivariable derivative-free optimization algorithms for unconstrained optimization problems are developed. A novel procedure for approximating the gradient of multivariable objective functions based on noncommutative maps is introduced. The procedure is based on the construction of an exploration sequence to specify where the objective function is evaluated and the definition of so-called gradient generating functions which are composed with the objective function, such that the procedure mimics a gradient descent algorithm. Various theoretical properties of the proposed class of algorithms are investigated and numerical examples are presented.

Index Terms—Adaptive control, extremum seeking, non-holonomic systems, optimization, optimization algorithms, perturbation methods.

I. INTRODUCTION

KEY ingredient in the solution of problems arising in machine learning, real-time decision-making, and control are sophisticated optimization algorithms. Hence, improving existing optimization algorithms and developing novel algorithms is of central importance in these areas. The optimization problems therein are often very challenging, i.e., they are high-dimensional, nonconvex, nonsmooth, or of stochastic nature. In addition, in some applications the evaluation of the objective to be optimized involves noisy measurements or the mathematical description of the objective is unknown. For this type of problems, a promising class of algorithms are derivative-free algorithms [1], which typically need only evaluations of the objective function for optimization. Due to the increasing computational

Manuscript received 2 June 2020; revised 7 June 2020, 18 March 2021, and 29 July 2021; accepted 7 November 2021. Date of publication 22 November 2021; date of current version 5 December 2022. This work was supported by the German Research Foundation DFG under Grant EB425/8-1. Recommended by Associate Editor Soon-Jo Chung. (Corresponding author: Jan Feiling.)

Jan Feiling is with the Institute for Systems and Control Theory, University of Stuttgart, 10435 Berlin, Germany (e-mail: jan.feiling@porsche.digital).

Mohamed-Ali Belabbas is with the ECE, University of Illinois at Urbana-Champaign, Urbana, IL 61801 USA (e-mail: belabbas@illinois.edu).

Christian Ebenbauer is with the Chair of Intelligent Control Systems, RWTH Aachen University, 52074 Aachen, Germany (e-mail: christian.ebenbauer@ic.rwth-aachen.de).

Color versions of one or more figures in this article are available at https://doi.org/10.1109/TAC.2021.3129741.

Digital Object Identifier 10.1109/TAC.2021.3129741

power and the generic applicability, derivative-free optimization algorithms have gained renewed interest in recent years, especially in the field of machine learning and control [2]–[10].

In this article, we propose a novel class of derivative-free optimization algorithms based on a concept introduced in [11]. The key idea is to use noncommutative maps to evaluate the objective function at certain points such that the composition of the maps approximates a gradient descent step. The class of proposed algorithms is built upon two main ingredients: An exploration sequence indicating where the objective is to be evaluated, and the (gradient) generating functions, which are composed with the objective function in such a way that an approximation of a gradient descent step is obtained. The resulting algorithms have several noteworthy properties. For example, the algorithms are sometimes able to overcome local minima and robust against noisy objective function evaluations. Such properties are also known from so-called extremum seeking algorithms (cf., e.g., [12]-[15]), which are related to our proposed algorithms [7], [11].

In our preliminary work [11], the algorithms were limited to optimization problems with one decision (optimization) variable or to a coordinatewise application of the gradient approximation scheme. Moreover, only a special case of generating functions were discussed and no full characterization was given. In another related work [16], the optimization procedure of [11] was extended to discrete-time extremum seeking problems, but still limited to one optimization variable.

More broadly related work in terms of gradient approximation schemes are, for example, finite difference approximations [17], [18], simultaneous perturbation stochastic approximations [5], and random directions stochastic approximations [19]; in [20] those approximation techniques are applied to the aforementioned extremum seeking problems. These methods are based on so-called sample averaging of function evaluations, i.e., the neighborhood of the current candidate solution is explored to approximate the local gradient of the optimization objective. In contrast, in the presented work, no numerical differentiation is performed to extract gradient information, instead a kind of numerical integration scheme is utilized to approximate first order-information.

The main contribution of this article is fourfold: 1) A constructive procedure for determining suitable exploration sequences for multivariable optimization problems is presented, 2) a general class of (gradient) generating functions is characterized,

0018-9286 © 2021 IEEE. Personal use is permitted, but republication/redistribution requires IEEE permission. See https://www.ieee.org/publications/rights/index.html for more information.

3) the so-called single and two-point algorithms in [11] and [16] are extended to the multivariable case, and 4) a toolbox is developed to easily design and apply the novel class of optimization algorithms to unconstrained optimization problems.

Notation: The set of real numbers equal or greater than kis denoted by $\mathbb{R}_{\geq k} = \{x \in \mathbb{R} \mid x \geq k\}$. The class of k-times continuously differentiable functions is denoted by $C^k(\mathbb{R}^n;\mathbb{R})$. $I \in \mathbb{R}^{n \times n}$ stands for the *n*-dimensional unit matrix, $\mathbb{1} \in \mathbb{R}^n$ for the *n*-dimensional all-one vector, and $e_i \in \mathbb{R}^n$ for the *i*th n-dimensional unit vector. The matrix $P \in \mathbb{R}^{n \times n}$ has the principal submatrix $P_{1:r} \in \mathbb{R}^{r \times r}$ with r < n. The bijective mapping $\pi:\{1,\ldots,n\}\to\{1,\ldots,n\}$ with $n\in\mathbb{N}$ denotes a permutation function. A sequence w_0, \ldots, w_{m-1} of length m is denoted by $\{w_\ell\}_{\ell=0}^{m-1}$. The ceiling and floor operator are defined as $|x| := \max\{k \in \mathbb{Z} \mid k \le x\} \text{ and } \lceil x \rceil := \min\{k \in \mathbb{Z} \mid k \ge x\},$ respectively. A function $f(x; \epsilon) : \mathbb{R}^n \times \mathbb{R} \times \mathbb{R}^n$ is said to be of order $\mathcal{O}(\epsilon)$, if for all compact sets $\mathcal{V} \subseteq \mathbb{R}^n$ there exist an $M \in \mathbb{R}_{>0}$ and $\bar{\epsilon} \in \mathbb{R}_{>0}$, such that for all $x \in \mathcal{V}$ and $\epsilon \in [0, \bar{\epsilon}]$, $|f(x;\epsilon)| \leq M\epsilon$. The operator mod takes to integers k and n and returns an integer $k \mod n$, equal to the remainder of the division of k by n. A compact set with center point $x^* \in \mathbb{R}^n$ radius $\delta \in \mathbb{R}_{>0}$ and denoted by $\mathcal{U}_{x^*}^{\delta} \subseteq \mathbb{R}^n$ is defined as $\{x \in \mathbb{R}^n : x \in \mathbb{R}^n : x$ $\mathbb{R}^n: ||xx^*||_2 < \delta\}.$

II. PROBLEM STATEMENT AND PRELIMINARIES

A. Problem Statement

In this article, we develop a class of algorithms to solve unconstrained minimization problems

$$\min_{x \in \mathbb{R}^n} J(x) \tag{1}$$

for which a closed form expression of $J:\mathbb{R}^n \to \mathbb{R}$ may be lacking, and only zero-order information in terms of function evaluations are available to find a local minimizer $x^* \in \mathbb{R}^n$ of J. The algorithms we propose are of the form

$$x_{k+1} = M_k^{\sqrt{h}}(x_k, J(x_k), \quad k \ge 0$$
 (2)

where we call $M_k^{\sqrt{h}}: \mathbb{R}^n \times \mathbb{R} \to \mathbb{R}^n$ the *transition map* and $h \in \mathbb{R}_{>0}$ is the step size. The main idea is to design the transition maps in such a way that for every $k \in \mathbb{N}$, the m-fold composition of these maps, i.e.,

$$x_{k+m} = \left(M_{k+m-1}^{\sqrt{h}} \circ \dots \circ M_k^{\sqrt{h}}\right) (x_k, J(x_k)) \tag{3}$$

approximates a gradient descent step, i.e.,

$$x_{k+m} = x_k - h\nabla J(x_k) + \mathcal{O}(h^{3/2})$$
 (4)

as visualized in Fig. 1.

Hereby, we impose the following structure for the transition maps

$$M_k^{\sqrt{h}}(x_k, J(x_k)) = x_k + \sqrt{h}\alpha_1 s_k (J(x_k))$$

$$+ \sqrt{h}\alpha_2 s_k \left(J\left(x_k + \sqrt{h}s_k(J(x_k))\right) \right)$$

$$s_\ell(J(x_k)) = f(J(x_k))u_\ell + g(J(x_k))v_\ell \tag{5}$$

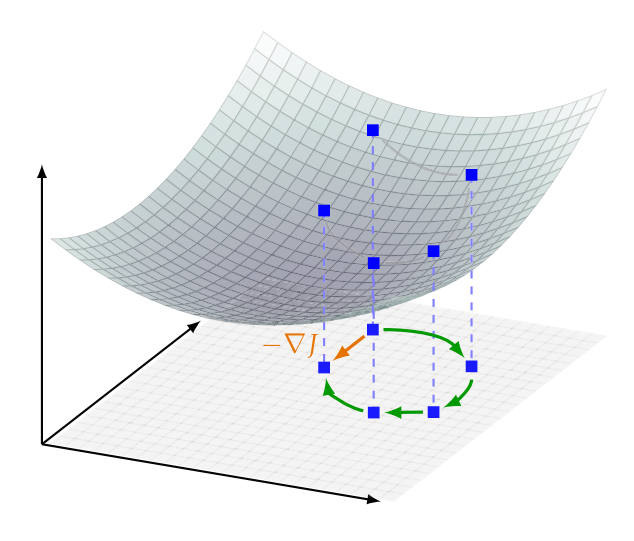


Fig. 1. Illustration of the presented optimization algorithms based on noncommutative maps. Effects of noncommutativity are utilized to approximate the negative gradient of the optimization objective in m steps (i.e., m=4 in this illustration).

with parameters $\alpha_1, \alpha_2 \in \mathbb{R}$, where $\alpha_1 + \alpha_2 \neq 0$. We call $s_\ell : \mathbb{R} \to \mathbb{R}^n$ the evaluation map, $f, g : \mathbb{R} \to \mathbb{R}$ the generating functions, and $u_\ell, v_\ell \in \mathbb{R}^n$ the m-periodic exploration sequences. Note that for $\alpha_2 \neq 0$, only two evaluations of J per iterations are necessary. We elaborate on the choice of this structure for the algorithm in Section III. The main goal of this work is to characterize and design

- 1) m-periodic exploration sequences u_{ℓ} , v_{ℓ} ; and
- 2) gradient generating functions f and g, such that (2) with transition map (5) yields (4).

We will at various points make the use of one or both of the following assumptions.

- A 1) The functions f, g are of class $C^2(\mathbb{R}, \mathbb{R})$ and the objective function J is of class $C^2(\mathbb{R}^n, \mathbb{R})$.
- A 2) The objective function J is radially unbounded and there exists an $x^* \in \mathbb{R}^n$, such that $\nabla J(x)^\top (x x^*) > 0$ for all $x \in \mathbb{R}^n \setminus \{x^*\}$.

We note that A 2) will not be required for the design of the algorithms, but only when we analyze their performance. The implementation of the algorithms, however, is not limited to the class of objective functions satisfying A 1).

B. Related Results

The structure of the transition map in (5) was introduced by the authors of the present work in [11] for one-dimensional problems. Therein, two cases were considered, specified by the parameter setting $[\alpha_1 \ \alpha_2] = [1 \ 0]$, as so-called *single-point* map

$$M_k^{\sqrt{h}}(x_k, J(x_k)) = E_k^{\sqrt{h}}(x_k, J(x_k)) := x_k + \sqrt{h}s_k(J(x_k))$$
(6)

and by $[\alpha_1 \ \alpha_2] = [1/2 \ 1/2]$, as so-called *two-point* map

$$M_k^{\sqrt{h}}(x_k, J(x_k)) = H_k^{\sqrt{h}}(x_k, J(x_k)) := x_k + \frac{\sqrt{h}}{2} \left[s_k \left(J(x_k) \right) \right]$$

$$+s_k \left(J(x_k + \sqrt{h}s_k (J(x_k)))\right)$$
. (7)

The algorithms relying on transition maps (6) and (7) are called single and two-point algorithm, respectively, reflecting that the number of function evaluations of J at each iteration is one and two. This type of map structure was inspired by the well-known Euler and Heun (trapezoidal) numerical integration methods, respectively, (thus the naming of the maps E and H), i.e., executing a single integration step with step size \sqrt{h} of the differential equation

$$\dot{x}(t) = s(J(x(t))) = f(J(x(t)))u(t) + g(J(x))v(t)$$
 (8)

with piecewise constant $m\sqrt{h}$ -periodic inputs $u(t), v(t) \in \mathbb{R}^n$ for $t \in [\ell\sqrt{h}, (\ell+1)\sqrt{h}]$ with $\ell \in \mathbb{N}$, yields (6) and (7), respectively. Note that (8) is well known as an approximate gradient descent flow in the context of extremum seeking control (cf. [12]). For a detailed explanation of the proposed class of algorithms and the continuous-time algorithm (8) plus how noncommutativity comes into play, we refer to [11] and [16].

For the coordinatewise descent case (see [11, Lemma 1 and Lemma 2]) the choice of exploration sequences

$$u_{\ell} = \bar{u}_{\ell}e_i$$
, $v_{\ell} = \bar{v}_{\ell}e_i$ with $i = \lfloor \ell/4 \rfloor \operatorname{mod}(n) + 1$

$$\bar{u}_{\ell} = \begin{cases} 1 & \ell = 0 \\ 0 & \ell = 1 \\ -1 & \ell = 2, \quad \bar{v}_{\ell} = \begin{cases} 0 & \ell = 0 \\ 1 & \ell = 1 \\ 0 & \ell = 2 \end{cases}$$

$$\bar{u}_{\ell-4} \text{ else}$$

$$(9)$$

$$\bar{v}_{\ell-4} \text{ else}$$

with m=4n leads to the evolution of x_k with $[\alpha_1 \ \alpha_2] = [1 \ 0]$, such that

$$x_{k+m} = x_k + h \{ ([f, g](J(x_k)) - \frac{1}{2} \frac{\partial (f^2 + g^2)}{\partial J} (J(x_k)) \} \nabla J(x_k) + \mathcal{O}(h^{3/2})$$
 (10)

and with $[\alpha_1 \ \alpha_2] = [1/2 \ 1/2]$, such that

$$x_{k+m} = x_k + h \{([f, g](J(x_k))\} \nabla J(x_k) + \mathcal{O}(h^{3/2})$$
 (11)

where $[f,g]:=rac{\partial g}{\partial J}f-rac{\partial f}{\partial J}g$ is the Lie bracket of f and g. A simple calculation shows that the term in brackets in (10) and (11) is identical to -1 for $f(J(x)) = \sin(J(x))$ and g(J(x)) = $\cos(J(x))$, hence (4) is recovered. The exploration sequence above is constructed in such a way that components of the gradient are approximated sequentially for the multidimensional setting, hence, coordinatewise. In Fig. 2, the exploration sequence and the gradient approximation is visualized for the scalar case $x_k \in \mathbb{R}$ (n = 1, m = 4). In summary, the existing procedure is limited and mimics a coordinatewise descent algorithm. Further, only a single exploration sequence was presented as well as a single pair of generating functions. There are, however, many ways to construct exploration sequences and generating functions, especially in the multivariable case. Since different exploration sequences and generating functions lead to different properties of the algorithm, it is the goal of this article to provide solutions for a flexible design and constructions of exploration

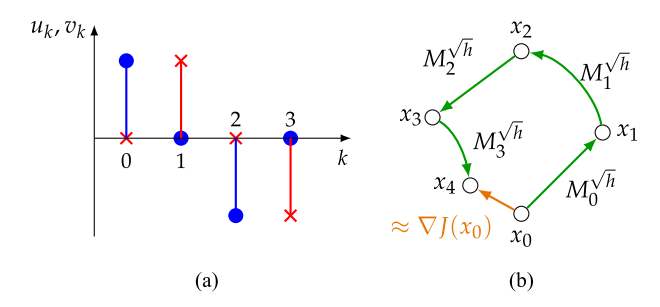


Fig. 2. (a) Periodic inputs u_k (•) and v_k (×) depicted for one period m=4 as specified in (9). (b) Noncommutative maps as in (5) with initial point x_0 .

sequences in the multivariable setting and to characterize a large class of generating functions.

III. MAIN RESULTS

A. Problem Statement Reformulation and Convergence

As described in Section II-A we aim to construct m-periodic exploration sequences u_ℓ and v_ℓ and generating functions f and g, such that (2) with transition map (5) yields (4). Our first result restates the problem in terms of solving a system of nonlinear equations. Since the sequences u_ℓ and v_ℓ are m-periodic, it suffices to determine the steps $k=0,\ldots,m-1$ in (5), i.e., one period of the exploration sequences.

Theorem 1: Let 1 hold. Then the mth step of the evolution of (2) with transition map (5) is given by

$$x_{m} = x_{0} + \sqrt{h(\alpha_{1} + \alpha_{2})}Y(f(J(x_{0})), g(J(x_{0})))W\mathbb{1}$$
$$+ h\tilde{Y}(f(J(x_{0})), g(J(x_{0})))T(W)$$
$$\times Y(f(J(x_{0})), g(J(x_{0})))^{\top}\nabla J(x_{0}) + \mathcal{O}(h^{3/2}).$$
(12)

Here, $W = [w_0 \ w_1 \ \cdots \ w_{m-1}] \in \mathbb{R}^{2n \times m}$ with $w_i = [u_i^\top \ v_i^\top]^\top$ is the exploration sequence matrix and $T(W) \in \mathbb{R}^{2n \times 2n}$ is given by

$$T(W) := \sum_{i=0}^{m-1} \left(\alpha_2 w_i w_i^\top + (\alpha_1 + \alpha_2)^2 \sum_{j=0}^{i-1} w_i w_j^\top \right). \quad (13)$$

Furthermore,
$$Y(f(z),g(z)):=\begin{bmatrix}f(z)I & g(z)I\end{bmatrix}\in\mathbb{R}^{n\times 2n}$$
 and $\tilde{Y}(f(z),g(z)):=\begin{bmatrix}\frac{\partial f}{\partial z}(z)I & \frac{\partial g}{\partial z}(z)I\end{bmatrix}=\frac{\partial}{\partial z}Y(f(z),g(z))\in\mathbb{R}^{n\times 2n}.$

The proof of Theorem 1 is given in Appendix B1. If there exist m-periodic exploration sequences $\{w_\ell\}_{\ell=0}^{m-1}$ (equivalently, an exploration sequence matrix W), and generating functions f and g, such that

$$\tilde{Y}(f(z), g(z))T(W)Y(f(z), g(z))^{\top} = -I \quad \forall z \in \mathbb{R}$$
 (14)

$$W1 = 0 \tag{15}$$

are satisfied, then (4) holds. Thus, this system of nonlinear ordinary differential equations (w.r.t. f(z) or g(z)) with unknown coefficients is key in designing the algorithm. The idea to solve this highly underdetermined system of equations is now to proceed in two steps as follows.

- Step 1: For a class of normal (skew-symmetric) matrices T_d , we construct exploration sequence matrices W, such that (15) and $T(W) = T_d$ hold.
- Step 2: We characterize gradient generating functions f, g and normal (skew-symmetric) matrices T_d , such that (14) holds.

These two constructions are presented in the following two subsections. We start with a remark on T(W) and the convergence result of the proposed algorithms.

Remark 1: To get a sense of (14) and the role of T(W), partition T(W) as

$$T(W) = \begin{bmatrix} T_{11}(W) & T_{12}(W) \\ T_{21}(W) & T_{22}(W) \end{bmatrix}$$
 (16)

with $T_{11}(W), T_{12}(W), T_{21}(W), T_{22}(W) \in \mathbb{R}^{n \times n}$. Note that $T_{11}(W)$ is defined solely by $\{u_\ell\}_{\ell=0}^{m-1}, T_{22}(W)$ solely by $\{v_\ell\}_{\ell=0}^{m-1}$, and $T_{12}(W)$ and $T_{21}(W)$ by both $\{u_\ell\}_{\ell=0}^{m-1}$ and $\{v_\ell\}_{\ell=0}^{m-1}$. Then (14) with (16) yields

$$\frac{\partial f}{\partial J}fT_{11} + \frac{\partial f}{\partial J}gT_{12} + \frac{\partial g}{\partial J}fT_{21} + \frac{\partial g}{\partial J}gT_{22} = -I \qquad (17)$$

where the arguments $J(x_0)$ of the maps f and g and their derivatives and W of T_{ij} with $i,j\in\{1,2\}$ are omitted for the sake of readability. By plugging $\{u_\ell\}_{\ell=0}^{m-1}$ and $\{v_\ell\}_{\ell=0}^{m-1}$ from (9), with W_1 and W_2 for $[\alpha_1 \ \alpha_2] = [1 \ 0]$ and $[\alpha_1 \ \alpha_2] = [1/2 \ 1/2]$, respectively, into (13), one obtains

$$T(W_1) = \begin{bmatrix} -I & -I \\ I & -I \end{bmatrix}$$
, and $T(W_2) = \begin{bmatrix} 0 & -I \\ I & 0 \end{bmatrix}$. (18)

Hence, the left hand side of (17) translates into the terms in the curly brackets in (10) and (11), respectively. A geometric interpretation of T(W) is discussed in Section IV-B.

Due to property (4), for example, semiglobal practical asymptotic convergence to the optimizer x^* can be established (see [21]):

Theorem 2: Let 1 and 2 hold. Assume that there exist generating functions f(J(x)) and g(J(x)) and an exploration sequence matrix W, such that (14) and (15) are satisfied. Then, for all $\delta_1, \delta_2 \in \mathbb{R}_{>0}$ with $\delta_2 < \delta_1$, there exist an $h^* \in \mathbb{R}_{>0}$ and $N(h) \in \mathbb{N}$, such that for all $h \in \{\bar{h} \mid 0 < \bar{h} < h^*\}$ and $x_0 \in \mathcal{U}_{x^*}^{\delta_1}$, it holds $x_k \in \mathcal{U}_{x^*}^{\delta_2}$ for all $k \geq N(h)$.

The proof of Theorem 2 follows along the lines of the proof of [11, Th. 2] by utilizing Theorem 3 in Appendix A and Theorem 1.

Remark 2: Theorem 2 is based on a constant step size h. Applying a variable decreasing step size h_k , but constant over a period of length m, i.e., $h_0 = h_1 = \cdots = h_{m-1}$, $h_m = h_{m+1} = \cdots = h_{2m-1}$, ..., with

$$\sum_{p=0}^{\infty} h_{pm} = \infty, \quad \sum_{p=0}^{\infty} h_{pm}^2 < \infty \tag{19}$$

e.g., $h_k = 1/(\lfloor k/m \rfloor + 1)$ (cf. [5, Prop. 1]) lead to a semiglobal asymptotic convergence result and a potential numerical performance improvement. Note that the requirement of periodically m constant steps preserves the $\mathcal{O}(\sqrt{h})$ -order terms in (12) (cf. proof of Theorem 3).

B. Exploration Sequences

In this part we characterize the conditions under which there exists an exploration sequence matrix W for a given T_d , such that $T(W) = T_d$ together with $W\mathbb{1} = 0$ are satisfied, hence, addressing Step 1 as stated above. The next lemma represents T(W), i.e., (13), in combination with (15) in a more compact form.

Lemma 1: Consider (13) and suppose the exploration sequence matrix $W \in \mathbb{R}^{2n \times m}$ satisfies (15). Then T(W) can be expressed as

$$T(W) = \mathbf{W} \, \mathbf{P} \, \mathbf{W}^{\top} \tag{20}$$

with $P \in \mathbb{R}^{m \times m}$ defined as

$$P = \begin{bmatrix} c_1 & c_2 & \cdots & c_2 & 0 \\ \alpha_2 & \ddots & \ddots & \vdots & \vdots \\ \vdots & \ddots & \ddots & c_2 & \vdots \\ \alpha_2 & \cdots & \alpha_2 & c_1 & 0 \\ 0 & \cdots & \cdots & 0 & 0 \end{bmatrix}$$
(21)

where $c_1 = 2\alpha_2 - (\alpha_1 + \alpha_2)^2$, $c_2 = \alpha_2 - (\alpha_1 + \alpha_2)^2$, and α_1, α_2 defined in (5).

The proof of Theorem 1 is given in Appendix B2. Consequently, when proceeding according to Steps 1 and 2 described in the section above, the key equations for the design of the exploration sequences are

$$WPW^{\top} = T_d$$

$$W1 = 0.$$
(22)

The following theorem, which provides a constructive design of the exploration sequence matrix W, is of central importance. It also provides structural insight in terms of obtaining lower bounds on the length (period) of the exploration sequence m, suitable choices of the parameters α_1 and α_2 and admissible structures for the desired target matrices T_d .

Theorem 3: Given α_1, α_2 and $T_d \in \mathbb{R}^{2n \times 2n}$. Suppose that either T_d is normal, $(2\alpha_2 - (\alpha_1 + \alpha_2)^2)(T_d + T_d^\top)$ positive definite, and Conjecture 1 (see below) is satisfied or that T_d is skew-symmetric with $2\alpha_2 - (\alpha_1 + \alpha_2)^2 = 0$. Then there exists an $m \ge \operatorname{rk}(T_d) + 1$, such that $W \in \mathbb{R}^{2n \times m}$ satisfies the system of equations (22).

The role of Conjecture 1 in Theorem 3 is discussed in Remark 3.

Conjecture 1: Let the skew-symmetric matrix $C(m) \in \mathbb{R}^{m \times m}$ be defined as

$$C(m) := A(m) + \epsilon(m+1)B(m) \tag{23}$$

$$A(m) := \begin{bmatrix} 0 & 1 & \cdots & 1 \\ -1 & \ddots & \ddots & \vdots \\ \vdots & \ddots & \ddots & 1 \\ -1 & \cdots & -1 & 0 \end{bmatrix} \in \mathbb{R}^{m \times m}$$
 (24)

$$B(m) := \mathbb{1}[0 \ 2 \ 4 \ \dots \ 2(m-1)] - (\mathbb{1}[0 \ 2 \ 4 \ \dots \ 2(m-1)])^T \in \mathbb{R}^{m \times m}$$
 (25)

with $\epsilon(m) = (m-1)^{-1}(1-m^{-1/2})$. Then for any $m \ge 2$, C(m) and C(m+1) satisfy the eigenvalue interlacing property (cf. Theorem 4 in Appendix A).

$$\omega_k^{m+1} > \omega_k^m > \omega_{k+1}^{m+1} \ge 0 \tag{26}$$

for $k=1,\ldots,\lfloor m/2\rfloor$, where $\pm \omega_k^m i$ are the eigenvalues of C(m), with $\{\omega_k^m\}_{k=1\ldots m}$ sorted in nondecreasing order in k for m fixed.

Remark 3: We verified numerically that Conjecture 1 is always true (we verified it up to dimension m=10000, see Theorem A), but a proof is still lacking. Further notice, that C(m) is part of the following equation:

$$\tilde{P}(m) = \left(P - \epsilon(m)(\mathbb{1}\mathbb{1}^{\mathsf{T}}P + P\mathbb{1}\mathbb{1}^{\mathsf{T}}) + \epsilon^{2}(m)\mathbb{1}\mathbb{1}^{\mathsf{T}}P\mathbb{1}\mathbb{1}^{\mathsf{T}}\right)_{1:m-1}$$

$$= \left(\frac{1}{2}(\alpha_{1} + \alpha_{2})^{2} - \alpha_{2}\right)I$$

$$+ \frac{1}{2}(\alpha_{1} + \alpha_{2})^{2}C(m-1)$$
(27)

with P in (21) and $\epsilon(m)$ defined in Conjecture 1. Note that the interlacing property (26) holds also for $\tilde{P}(m)$, since it is arranged by a scaled unit matrix and the skew-symmetric matrix C(m-1) (cf. [22]). The interlacing property of $\tilde{P}(m)$ is utilized in the proof of Theorem 3.

The proof of Theorem 3 is constructive and presented in Appendix B3, where in particular in (76), Conjecture 1 enters. A step-by-step construction of W for a given T_d including a MATLAB toolbox is provided in [23]. Moreover we obtain as a corollary (which follows by the proof of Theorem 3).

Corollary 1: If $2\alpha_2 - (\alpha_1 + \alpha_2)^2 = 0$ and T_d skew-symmetric, then there always exists an $W \in \mathbb{R}^{2n \times m}$ with $m = \text{rk}(T_d) + 1$.

Remark 4: It is worthwhile to point out an interesting connection between the equations in (22) and nonlinear control theory, i.e., the controllability of the so-called nonholonomic integrator. Suppose $\{w_\ell\}_{\ell=0}^{m-1}$ is a solution of (22), then it can be verified by direct calculations (see also proof of Theorem 1 in Appendix B2) that it is also a solution of the two point boundary value problem

$$y_0 = 0, \ Z_0 = 0, \ y_m = 0, \ Z_m = T_d$$

$$y_{k+1} = y_k + w_k$$

$$Z_{k+1} = Z_k + (\alpha_1 + \alpha_2)^2 w_k y_k^\top + \alpha_2 w_k w_k^\top$$
 (28)

with $k=0,\ldots,m-1$, states $y_k\in\mathbb{R}^{2n},\,Z_k\in\mathbb{R}^{2n\times 2n}$, input $w_k\in\mathbb{R}^{2n}$, and vice versa. In particular with W1=0, i.e.,

$$w_{m-1} = -\sum_{i=0}^{m-2} w_i, (28) \text{ translates into}$$

$$y_0 = 0, \quad Z_0 = 0, \quad Z_{m-1} = T_d$$

$$y_{k+1} = y_k + w_k$$

$$Z_{k+1} = Z_k + \alpha_2 w_k y_k^\top + (\alpha_2 - (\alpha_1 + \alpha_2)^2) y_k w_k^\top + (2\alpha_2 - (\alpha_1 + \alpha_2)^2) w_k w_k^\top.$$

$$(29)$$

Considering now the case $[\alpha_1 \ \alpha_2] = [1/2 \ 1/2]$ shows that (29) is the state-transition of the generalized discrete-time non-holonomic integrator [24] with given initial and final states. Problem (28) with $[\alpha_1 \ \alpha_2] = [1 \ 0]$ has a similar structure. Hence, Theorem 3 provides an explicit solution to this state transition problem. Moreover, this viewpoint underlines the relationship to noncommutative maps and flows as indicated in Section II-B (Fig. 2). Another, more geometric, interpretation of (22) is also provided in Section IV-B.

C. Gradient Generating Functions

This part addresses Step 2, i.e., solving the (functional) (14) for f,g, and $T_d \in \mathbb{R}^{2n \times 2n}$ with $T(W) = T_d$. First, solutions (T_d,f,g) for the parameter setting $2\alpha_2 - (\alpha_1 + \alpha_2)^2 = 0$ are presented.

Theorem 4: Let $2\alpha_2 - (\alpha_1 + \alpha_2)^2 = 0$ and T_d skew-symmetric, then (14) is satisfied by the following triples (T_d, f, g) , where $a, b \in \mathbb{R}_{>0}$ and $c, \phi \in \mathbb{R}$:

$$T_{d} = \begin{bmatrix} 0 & -I \\ I & 0 \end{bmatrix}$$

$$g(z) = -f(z) \int f(z)^{-2} dz, f : \mathbb{R} \to \mathbb{R}$$

$$T_{d} = \begin{bmatrix} aQ & -I \\ I & bQ \end{bmatrix}, Q = -Q^{\top}$$

$$f(z) = a^{-1/2} \sin\left(\sqrt{ab}z + \phi\right)$$

$$g(z) = b^{-1/2} \cos\left(\sqrt{ab}z + \phi\right)$$

$$T_{d} = \begin{bmatrix} aQ & -I \\ I & -bQ \end{bmatrix}, Q = -Q^{\top}$$

$$f(z) = \pm a^{-1/2} \cosh\left(\sqrt{ab}z + \phi\right)$$

$$g(z) = \mp b^{-1/2} \sinh\left(\sqrt{ab}z + \phi\right)$$

$$G(z) = \mp b^{-1/2} \sinh\left(\sqrt{ab}z + \phi\right)$$

$$T_{d} = \begin{bmatrix} Q & -I \\ I & 0 \end{bmatrix}, Q = -Q^{\top}$$

$$(32)$$

(33)

 $f(z) = \pm \sqrt{a}, \ g(z) = \mp \frac{z}{\sqrt{a}}$

 $T_d = \begin{vmatrix} 0 & -I \\ I & O \end{vmatrix}, \ Q = -Q^{\top}$

$$f(z) = \pm \frac{z}{\sqrt{a}}, \ g(z) = \pm \sqrt{a}$$

$$T_d = \begin{bmatrix} 0 & -I - Q \\ I - Q & 0 \end{bmatrix}, \ Q = -Q^{\top}$$

$$f(z) = \pm \frac{1}{\sqrt{a}} e^{-\frac{a}{2}z}, \ g(z) = \mp \frac{1}{\sqrt{a}} e^{\frac{a}{2}z}$$

$$T_d = \begin{bmatrix} aQ & -I - cQ \\ I - cQ & bQ \end{bmatrix}, \ Q = -Q^{\top}$$

$$f(z) = \sqrt{\frac{b}{ab - c^2}} \sin\left(\sqrt{ab - c^2}z + \phi\right)$$

$$g(z) = b^{-1/2} \cos\left(\sqrt{ab - c^2}z + \phi\right)$$
(36)

In addition, for each T_d in (30)–(36) there exists an W, such that $T(W) = T_d$ in (13). In (36), we require that a, b > c.

Remark 5: Every pair f, g in (31)–(36) satisfy (30), hence, these generating functions are valid for the given T_d in (30), too. The advantage of the specified T_d 's are discussed in Section IV-B.

Remark 6: Consider the indefinite integral in (30). Let $F: \mathbb{R}^n \to \mathbb{R}$ be an antiderivative of $f(z)^{-2}$. Then so is $F + \bar{c}$ for any $\bar{c} \in \mathbb{R}$. Set $g(z) = -f(z)(F(z) + \bar{c})$. The constant \bar{c} is chosen, such that g'(z)f(z) - f'(z)g(z) = -1.

The proof of Theorem 4 is given in Appendix B4. Solutions (T_d, f, g) of (14) for the parameter setting $2\alpha_2 - (\alpha_1 + \alpha_2)^2 \neq 0$ are presented next.

Theorem 5: Let $T_d \in \mathbb{R}^{2n \times 2n}$ be normal and $(2\alpha_2 - (\alpha_1 + \alpha_2)^2)(T_d + T_d^\top)$ be positive definite, then (14) is satisfied by the following triples (T_d, f, g) , where $r : \mathbb{R} \to \mathbb{R}_{>0}$, $a \in \mathbb{R} \setminus \{0\}$, $b \in \mathbb{R}_{>0}$, and $\phi \in \mathbb{R}$:

$$T_{d} = \begin{bmatrix} aI & -I \\ I & aI \end{bmatrix}, \ a(2\alpha_{2} - (\alpha_{1} + \alpha_{2})^{2}) > 0$$

$$f(z) = \sqrt{r(z)}\sin(\varphi(z)), \ g(z) = \sqrt{r(z)}\cos(\varphi(z))$$

$$\varphi(z) = \frac{a}{2}\ln(r(z)) + \int \frac{1}{r(z)}dz + \phi$$

$$T_{d} = \begin{bmatrix} Q & -I \\ I & Q \end{bmatrix}$$

$$(2\alpha_{2} - (\alpha_{1} + \alpha_{2})^{2})(Q + Q^{\top})$$
(37)

pos. def. and normal

$$f(z) = b^{-1/2} \sin(bz + \phi)$$

$$g(z) = b^{-1/2} \cos(bz + \phi).$$
 (38)

In addition for every T_d in (37)–(38) there exists an W, such that $T(W) = T_d$ in (13).

The proof of Theorem 5 is given in Appendix B5.

Remark 7: The list of triples (T_d, f, g) in Theorem 4 is essentially exhaustive, save for some scaled version of the presented cases. A case-by-case study is presented in the proof of

Algorithm 1: Derivative-Free Optimization Algorithm With Noncommutative Maps.

```
Input: x_0, h, \alpha_1, \alpha_2, f(J(\cdot)), g(J(\cdot)), T_d,
       \sigma_i (i = 1, \dots, \text{rk}(T_d)), stop criterion
       Calculate W and m as described in Appendix C in [23]
 3:
 4:
       while stop criterion is not fulfilled do
 5:
          \ell = k \mod (m) + 1
          e_{\ell} = [0_{\ell}, 1, 0_{n-1-\ell}]^{\top}
 6:
          Y(J(x_k)) = [f(J(x_k))I \ g(J(x_k))I]
 7:
          \hat{x}_k = x_k + \sqrt{h}Y(J(x_k))We_\ell
 8:
          Y(J(\hat{x}_k)) = [f(J(\hat{x}_k))I \ g(J(\hat{x}_k))I]
 9:
10:
          x_k + \sqrt{h}(\alpha_1 Y(J(x_k)) + \alpha_2 Y(J(\hat{x}_k)))We_{\ell}
11:
12:
       end while
13:
       return [x_0, x_1, \ldots]
```

Theorem 4 in Appendix B4. Whereas the list of triples (T_d, f, g) in Theorem 5 is not exhaustive (cf. Appendix B5).

Theorem 4 and Theorem 5 together with Theorem 3 solve (14) and (15), and thus, ensure the existence of a exploration sequence W. Hence, a gradient descent step is approximated by the proposed algorithm (2) with transition maps (5).

IV. ALGORITHM, PARAMETERS, AND NUMERICAL RESULTS

In this section we present some numerical studies of the proposed class of algorithms. We carry out simulations and discuss how various choices of T_d , of the singular values of W, of the sequence length (period) m, or of the parameters α_1, α_2 influence the qualitative behavior of the algorithm. Further, a numerical approach to construct the exploration sequences using nonlinear programming is presented.

We start by summarizing the proposed optimization algorithm and the involved parameters.

A. Algorithm and Parameters

The design parameters and functions involved in the proposed algorithm are as follows.

- 1) Map parameters $\alpha_1, \alpha_2 \in \mathbb{R}$ with $\alpha_1 + \alpha_2 \neq 0$.
- 2) Gradient generating functions $f, g : \mathbb{R} \to \mathbb{R}$.
- 3) Matrix T_d and exploration sequence matrix W, in particular singular values σ_i , $i = 1, ..., \text{rk}(T_d)$ of W.
- 4) Step size h > 0.

Hence, algorithm (2) with (5) is defined in terms of W as follows.

Notice that $Y(J(x_k))$ is a $n \times 2n$ matrix. Moreover, if $\alpha_2 = 0$, then line 8 and 9 in Algorithm 1 can be skipped.

In the following we discuss the influence of the design parameters on the algorithm's behavior. Additionally, a set of parameters working well in generic situations, which can then be used as a starting point to obtain optimized parameters for a particular application, is provided.

- 1) Map Parameters $\alpha_1,\ \alpha_2$: The parameters weigh $Y(J(x_k))$ and $Y(J(\hat{x}_k))$ in Algorithm 1, respectively. In particular, they can be utilized to choose between a single-point $(\alpha_2=0)$ or a two-point algorithm. They are to be normalized according to $\alpha_1+\alpha_2=1$ and to tune according to the ratio of α_1,α_2 , while utilizing the step size h to tune the convergence speed. Moreover, the choice of α_1,α_2 restricts the choice of T_d to be skew-symmetric for $2\alpha_2-(\alpha_1+\alpha_2)^2=0$ and otherwise normal (cf. Theorem 4 and Theorem 5). In practice, the parameter sets we found providing the best performance were $[\alpha_1,\alpha_2]=[1\ 0]$ for the single-point and $[\alpha_1,\alpha_2]=[1/2\ 1/2]$ for the two-point gradient-approximation scheme.
- 2) Generating Functions f, g: The generating functions comprise a scaling of the objective evaluated at x_k and \hat{x}_k as stated in Algorithm 1. Various choices are presented in Theorem 4 and Theorem 5; depending on α_1, α_2 . Often we have chosen f, g as sinusoidal functions, since the algorithm showed a very stable behavior for that cases. Note that high function values of f, g or if f, g scale arbitrarily large with $J(x_k)$, the algorithm performs large steps which may cause instabilities. In the case of bounded functions, such as sinusoidal functions, (arbitrarily) large steps sizes are avoided. Further, if J, f, g vanish at a minimum x^* , asymptotic convergence to x^* (instead of practical convergence) has been observed in our studies.
- 3) Exploration Sequence Matrix W and T_d : The exploration sequence matrix W depends on the choice of T_d , specifically on the eigenvalues of T_d . A step-by-step construction of W based on the algorithm parameters is presented in [23]. As explained in this construction, the singular values of W can be chosen (see Theorem 2 below), hence this degree of freedom can be used in the algorithm tuning. As shown in numerical examples below, smaller singular values lead to smoother trajectories, but more steps (larger m) are needed to perform one gradient approximation step. There exists a set of optimal singular values in the sense of minimal number of steps m, which is $m = \operatorname{rk}(T_d) + 1$. Therewith, the choice of T_d influences the lower bound on m (see Theorem 3 below). Note that minimal sequence length m does not always lead to the fastest convergence behavior.
- 4) Step Size h: The approximated gradient is scaled with the step size h, and hence, h influences the speed of convergence, as well as the area of exploration around x_k . As stated in Theorem 2 there exists an upper bound on h, such that semiglobal practical asymptotic convergence [if (A1) and (A2) holds] is ensured. In our numerical studies, h is often chosen as $0.001 \le h \le 0.5$.

Corollary 2: In the case $2\alpha_2-(\alpha_1+\alpha_2)^2=0$, the singular values $\sigma_{2\ell-1},\sigma_{2\ell},\,\ell=1,\ldots,\lceil \mathrm{rk}(T_d)/2\rceil$, of W can be chosen arbitrarily. Otherwise, the singular values of W have to satisfy $\sigma_{2\ell-1}=\sigma_{2\ell}$ and

$$T_d = \begin{bmatrix} \operatorname{diag}([\gamma_1 \cdots \gamma_n]) & -I \\ I & \operatorname{diag}([\gamma_1 \cdots \gamma_n]) \end{bmatrix}$$
(39)

with

$$\gamma_{\ell} = \left(\alpha_2 - \frac{1}{2}(\alpha_1 + \alpha_2)^2\right)\sigma_{2\ell-1}^2.$$
(40)

Proof: Following directly from the proof of Theorem 3 in Appendix B3. Specifically, T_d in (39) satisfies (38) and (40) corresponds to (73).

Corollary 3: The minimal number of steps to approximate a gradient according to (2)–(5) and using the T_d 's in Theorem 4 and Theorem 5 is m=n+1.

Proof: Since the first n rows of each T_d in Theorem 4 and Theorem 5 are linearly independent, we know $\min\{\operatorname{rk}(T_d)\} \geq n$. This implies with Theorem 3 that $m \geq n+1$.

Remark 8: A gradient step is a approximated in m = n + 1 steps for T_d as specified in (31) and Q with elements $\{q_{ij}\}_{i,j=1}^{2n}$, such that

$$q_{ij} = \begin{cases} 1 & \text{if } i+j = 2n+1, \ i > j \\ -1 & \text{if } i+j = 2n+1, \ i < j \\ 0 & \text{else} \end{cases}$$
 (41)

holds, while the singular values $\sigma_{2\ell-1}$, $\sigma_{2\ell}$ of W satisfy (75) for $\ell=1,\ldots,\lceil n/2\rceil$.

B. Numerical Results

In the following, various simulation results are presented to illustrate the influence of the algorithm parameters, i.e., matrix T_d , singular values σ_k , $k=1,\ldots,r$, of W and map parameters α_1,α_2 . For the sake of visualization, we focus on examples with n=2.

An extensive benchmarking study, including the best choice of parameters for certain classes of the objective, is beyond the scope of this article and carried out in ongoing and future work. Hence, we keep f,g, (sinusoidal) and h fixed and provide only a limited number of simulation examples to get some qualitative insight in the degrees of freedom and how they influence the algorithms behavior. In the figures below, we show trajectories and the exploration sequences. In addition, we provide a geometric interpretation and a visualization of the matrix T(W) which is of interest by its own and which is explained next.

The values of the components of T(W) in (13) for $[\alpha_1 \ \alpha_2] = [1/2 \ 1/2]$, i.e.,

$$T(W)_{pq} = \sum_{i=0}^{m-1} \sum_{j=0}^{i-1} \frac{1}{2} e_p^{\top} w_i w_i^{\top} e_q + e_p^{\top} w_i w_j^{\top} e_q$$
 (42)

with $p,q=1,\ldots,2n$, where the index pq specifies the element of T(W) in the pth row and qth column, can be interpreted as the projected areas spanned by the exploration sequences $\{e_p^\top w_\ell\}_{\ell=0}^{m-1}, \ \{e_q^\top w_\ell\}_{\ell=0}^{m-1}.$ The net area A_{pq} of an n-sided polygon with corner points $(x_{p,i},y_{q,i})\in\mathbb{R}^2, i=0\ldots n-1$ and $p,q=1,\ldots,2n$, known as Shoelace or Gauss area formula [25] is obtained as a special case of Green's theorem and is given by

$$A_{pq} = \frac{1}{2} \sum_{i=0}^{n-1} (x_{p,i+1} y_{q,i} - x_{p,i} y_{q,i+1})$$
 (43)

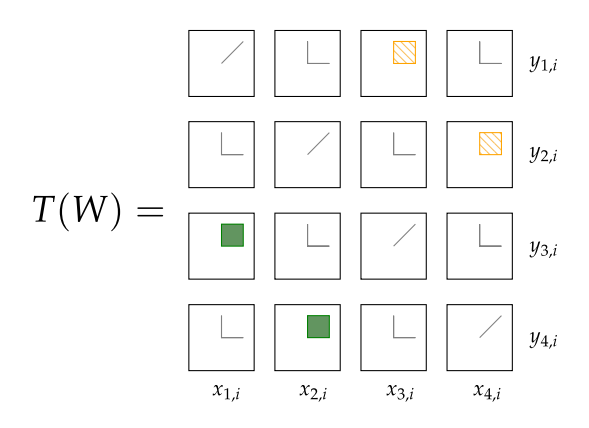


Fig. 3. Generated areas of the exploration sequence $\{w_k\}_{k=0}^{m-1}$ in (9) for $T(W) \in \mathbb{R}^{2n \times 2n}$ as given in (42) for n=2. Hence, $T(W)_{1,3} = T(W)_{2,4} = -1$, $T(W)_{3,1} = T(W)_{4,2} = 1$, and the rest 0. The filled green areas () have an area surface value of 1, the striped orange area () of -1, and the rest of 0. The coordinates of each subplot are given by $x_{p,i}$ and $y_{q,i}$ defined in (44) for $p,q=1,\ldots,2n$.

with $x_{p,0} = x_{p,n} = 0$ and $y_{q,0} = y_{q,n} = 0$. In Theorem 6 (Appendix A) we show that (43) is equivalent to (42) for

$$x_{p,i} = \sum_{k=0}^{i-1} e_p^{\top} w_k, \ y_{q,i} = \sum_{k=0}^{i-1} e_q^{\top} w_k.$$
 (44)

This geometric interpretation is not surprising in the light of Remark 4 and the area generating rule appearing in the study of nonholonomic systems [26]. In particular, (43) represents a (double) iterated summation over the exploration sequence. In the continuous-time setting, this would correspond to double iterated integrals (or in general k-fold iterated integrals, which are called the signature of a path) and which play a fundamental role in nonholonomic control systems. Note that for $[\alpha_1 \ \alpha_2] \neq [1/2 \ 1/2]$, (43) with (44) does not hold. However, we believe it is related to some kind of weighted area.

To illustrate this geometric interpretation, the exploration sequence in (9) with $[\alpha_1 \ \alpha_2] = [1/2 \ 1/2]$ generates T(W) as depicted in Fig. 3, where the singular values of W are $\sigma_1 = \sigma_2 = \sigma_3 = \sigma_4 = \sqrt{2}$. Obviously and as presented in the sequel, the singular values of W influence the shape of the areas and give rise to various interpretations of the algorithms behavior.

Simulation 1: In the first simulation setup we consider the objective $J(x) = \|x - [1 \ 2]^\top\|_2^2$ and setting $f(J(x)) = \sin(J(x))$, $g(J(x)) = \cos(J(x))$, $[\alpha_1 \ \alpha_2] = [1/2 \ 1/2]$, T_d as in (30), h = 0.05, and $x_0 = [0 \ 1]^\top$. The simulation results for two different choices of singular value pairs are depicted in Fig. 4. On the one hand $\sigma_1 = \sigma_2 = \sigma_3 = \sigma_4 = 1$ yields m = 8 and on the other hand $\sigma_1 = \sigma_3 = 1.5$, $\sigma_2 = \sigma_4 = 0.2$ results in m = 21. In the latter case the areas with net area value ± 1 have an elongated elliptical shape, which yield a small amplitude of $\{v_k\}_{k=0}^{m-1}$ and therefore a small steady-state amplitude since $\sin(J(x^*)) = 0$ and $\cos(J(x^*)) = 1$ [cf. (5)]. Concluding, the amplitude of $\{e_i^\top w_\ell\}_{\ell=0}^{m-1}$ is proportional to σ_i with $i = 1, \ldots, 2n$ for this choice of T_d .

Simulation 2.: In the second simulation study, we consider the same setup as in Simulation 1, but choose T_d as in (31) with Q as specified in the proof of Theorem 3. The simulation results

for two different choices of singular values pairs are depicted in Fig. 5. On one hand $\sigma_1 = \sigma_2 = 2$ results in m = 4 and on the other hand $\sigma_1 = \sigma_2 = 0.2$ in m = 154. The singular values can be interpreted as a kind of energy measurement of the exploration sequence, and therefore in the latter case, m is much larger, but reveals a smoother behavior. Moreover, σ_i influences the amplitude of $\{e_{2i-1}^{\top}w_\ell\}_{\ell=0}^{m-1}$ and $\{e_{2i}^{\top}w_\ell\}_{\ell=0}^{m-1}$ for $i=1,\ldots,n$ for the given choice of T_d , compared to the previous simulation example. However, due to space limitations we omit the plots for $\sigma_1 \neq \sigma_2$.

Interestingly, as observed in Figs. 4 and 5(d) and (h), the areas of $T(W)_{ij}$ for $(i,j) \in \{(1,2),(2,1)\}$ and $(i,j) \in \{(3,4),(4,3)\}$ have the same shape as the last m steps of x_k .

Simulation 3.: Consider the same setup as in Simulation 1, but choosing $[\alpha_1 \ \alpha_2] = [1 \ 0]$ and T_d as described in (39). Choosing $\sigma_1 = \sigma_2 = \sigma_3 = \sigma_4 = 1$ results in the behavior depicted in Fig. 6(a)–(c), which is similar to the behavior from Fig. 4(a)–(d), where m=8, too. On the one hand, the number of evaluations of the objective J is reduced by half when compared to Simulation 1. On the other hand, in this parameter setup, the choice of singular values is restricted to $\sigma_1 = \sigma_2$ and $\sigma_3 = \sigma_4$, hence, a behavior as in Fig. 4(e)–(h) cannot be achieved. However, reducing $\sigma_3 = \sigma_4$ to 0.4 yields a scaling in the coordinate directions as illustrated in Fig. 6(d)–(f).

Simulation 4.: In this simulation scenario we consider the cost function $J(x) = \|x - [1\ 2]^\top + 0.5\sin(10\pi x)\|^2$, i.e., an objective with many local minima. We define $f(J(x)) = \sin(J(x))$, $g(J(x)) = \cos(J(x))$, $[\alpha_1\ \alpha_2] = [1/2\ 1/2]$, h = 0.05, and $x_0 = [1\ 2]^\top$. The simulation results with T_d as in Simulation 2 and $\sigma_1 = \sigma_2 = 1$ are depicted in Fig. 7. As motivated in the introduction, the proposed algorithm is able to overcome local minima and converges into a neighborhood of the global minimum. Due to the definition of the maps $M_k^{\sqrt{h}}$, the gradient of J is gained by a procedure similar to numerical integration. It has been observed in simulations that this procedure is numerically more stable than numerical differentiation (finite differences). In summary, this integrating behavior has the effect to even and flatten out local minima and noise, respectively, (cf. [7]).

Simulation 5.: One of the key advantages of derivative-free optimization is demonstrated, namely, to deal with nonsmooth objectives. To this end, in its ability to a simulation experiment, the cost function is set to $J(x) = \|x\|$. We use the same algorithm parameters as in Simulation 2, i.e., $f(J(x)) = \sin(J(x))$, $g(J(x)) = \cos(J(x))$, $[\alpha_1 \ \alpha_2] = [1/2 \ 1/2]$, h = 0.05, and $x_0 = [1 \ 2]^{\top}$ with T_d as in (31), Q specified in Theorem 3, and singular values $\sigma_1 = \sigma_2 = 0.4$. The algorithm's behavior is depicted in Fig. 8. Since no first-order information (derivatives) needs to be competed, the algorithm is, as expected, converging to the local minima.

Remark 9: It is worth to mention that a very promising generating function class is

$$f(z) = \sqrt{z}\sin(\ln(z)\mu), \ g(z) = \sqrt{z}\cos(\ln(z)\mu) \tag{45}$$

with $\mu \in \mathbb{R}_{>0}$, which belong to the setting of (30) and (37) (with some adaptions). Specifically, the Lie bracket between the generating functions results in $[f, g](z) = -\mu$, i.e., it holds

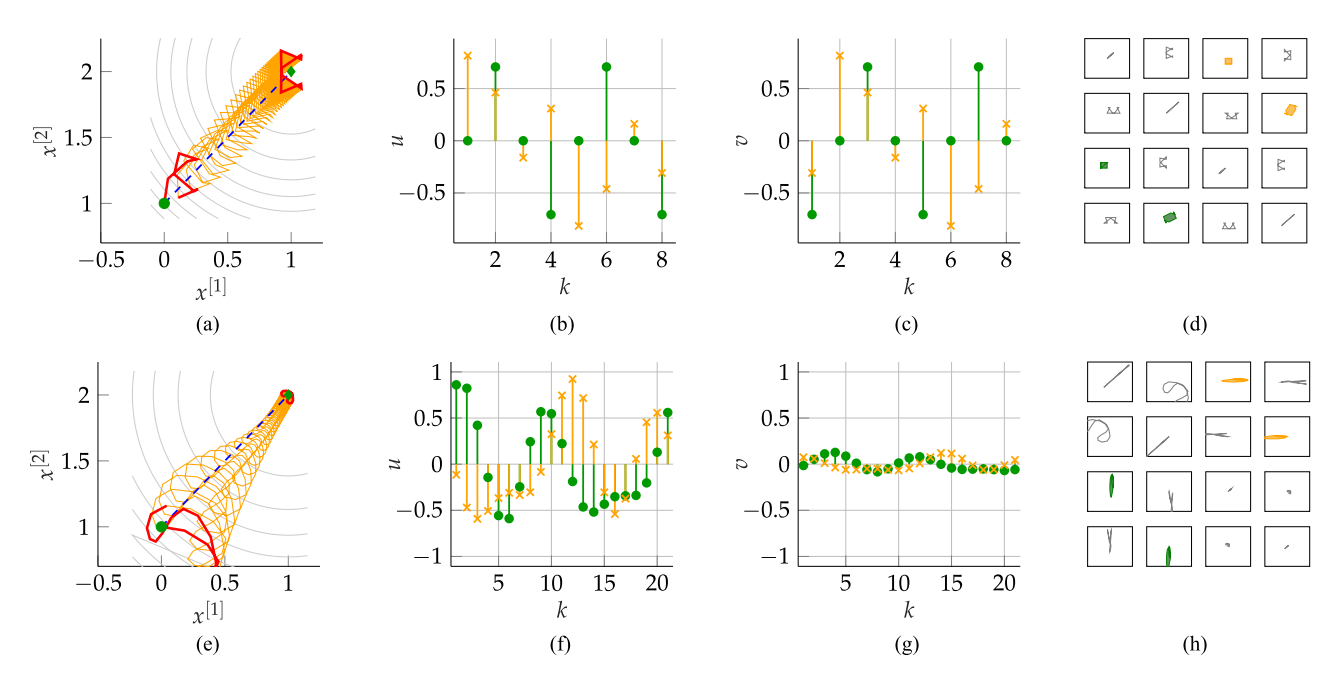


Fig. 4. Illustration of the algorithm's behavior (setup as in Simulation 1) with T_d as in (30) and singular values $[\sigma_1 \ \sigma_2 \ \sigma_3 \ \sigma_4] = [1 \ 1 \ 1 \ 1]$ (top) and $[\sigma_1 \ \sigma_2 \ \sigma_3 \ \sigma_4] = [1 \ 1 \ 0.2 \ 1.5 \ 0.2]$ (bottom) of the exploration matrix W. In (a) and (e) the trajectories x_k (__), the first and last m steps (__), the exact gradient descent algorithm (__), initial state x_0 (•), and optimizer x^* (•) are depicted. The plots (b) and (f) and (c) and (g) show the exploration sequence $\{u_k\}_{k=0}^{m-1}$ and $\{v_k\}_{k=0}^{m-1}$, respectively, where (•) is the first and (×) the second component. In (d) and (h) T(W) in form of the areas generated by $\{w_k\}_{k=0}^{m-1}$ is visualized, where the filled green areas (\blacksquare) have an area surface value of 1, the striped orange areas (\square) of -1, and the rest of 0.

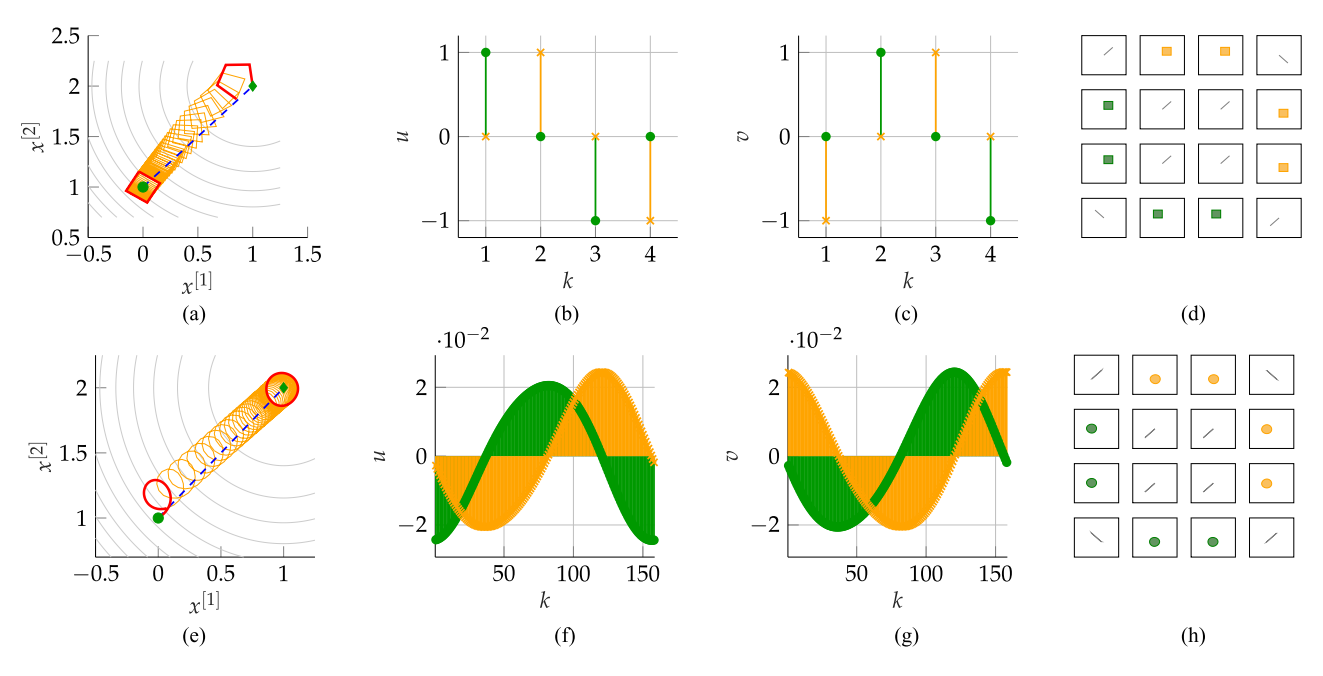


Fig. 5. Illustration of the algorithm's behavior (setup as in Simulation 2) with T_d as in (31) and singular values $[\sigma_1 \ \sigma_2] = [2 \ 2]$ (top) and $[\sigma_1 \ \sigma_2] = [0.2 \ 0.2]$ (bottom) of the exploration matrix W. In (a) and (e) the trajectories x_k (__), the first and last m steps (__), the exact gradient descent algorithm (__), initial state x_0 (__), and optimizer x^* (\P) are depicted. The plots (b) and (f) and (c) and (g) show the exploration sequence $\{u_k\}_{k=0}^{m-1}$ and $\{v_k\}_{k=0}^{m-1}$, respectively, where (__) is the first and (X) the second component. In (d) and (h) T(W) in form of the areas generated by $\{w_k\}_{k=0}^{m-1}$ is visualized, where filled green area (X) have an area surface value of 1, the striped orange area (X) of X0 or X1.

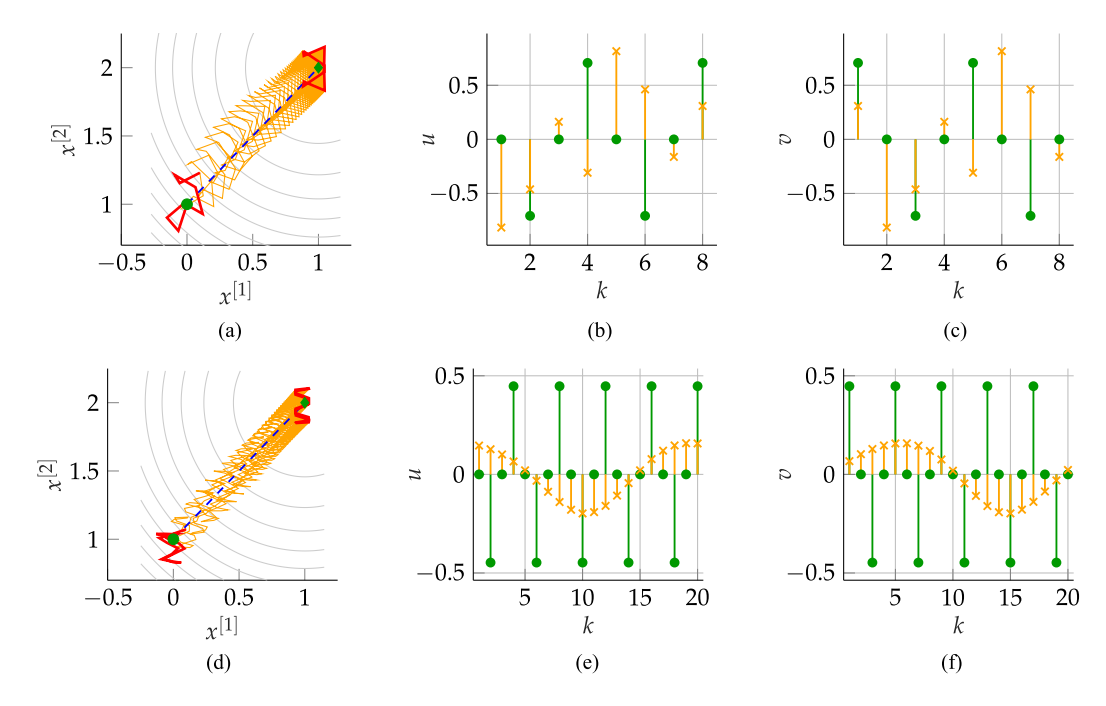


Fig. 6. Illustration of the algorithm's behavior (setup as in Simulation 3) with T_d as in (39) with singular values $[\sigma_1 \ \sigma_2 \ \sigma_3 \ \sigma_4] = [1 \ 1 \ 1 \ 1]$ (top) and $[\sigma_1 \ \sigma_2 \ \sigma_3 \ \sigma_4] = [1 \ 1 \ 0.4 \ 0.4]$ (bottom) of the exploration matrix W. In (a) and (d), the trajectories x_k (__), the first and last m steps (__), the exact gradient descent algorithm (__), initial state x_0 (•), and optimizer x^* (•) are depicted. The plots (b) and (c) and (f) show the exploration sequence $\{u_k\}_{k=0}^{m-1}$ and $\{v_k\}_{k=0}^{m-1}$, respectively, where (•) is the first and (×) the second component.

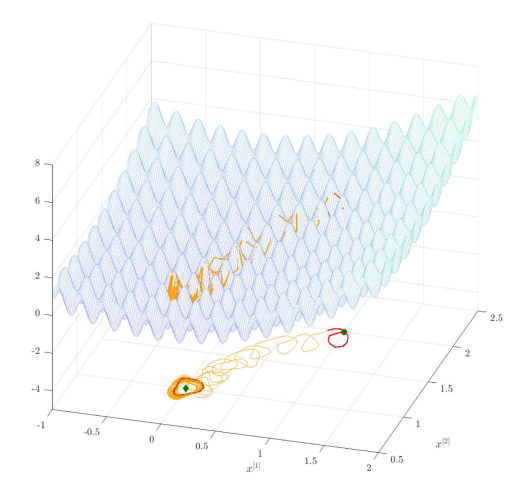
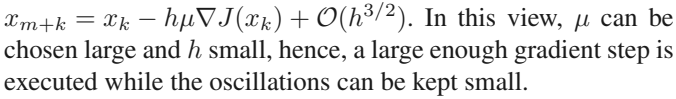


Fig. 7. Illustration of the algorithms behavior (setup as in Simulation 4) for T_d as in (31) and singular values $[\sigma_1 \ \sigma_2] = [1 \ 1]$ of exploration matrix W. The trajectories x_k (__), the first and last m steps (__), the initial state x_0 (•), and the optimizer x^* (•) are depicted.



Detailed implementations and a MATLAB toolbox can be found in [23].

C. Exploration Sequences Via Nonlinear Programming

Besides the construction of the exploration sequence as described in the proof of Theorem 3 in Appendix B3 and the

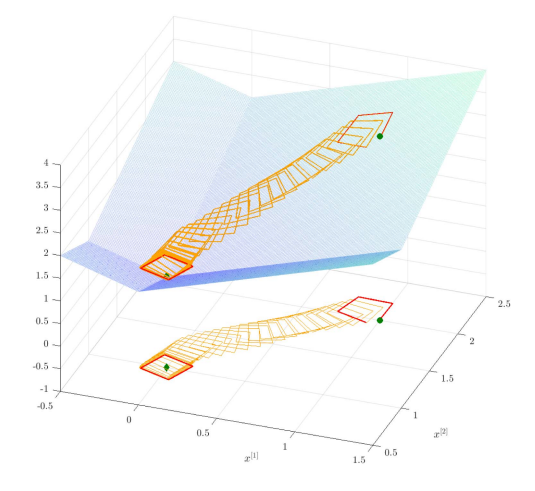


Fig. 8. Illustration of the algorithm's behavior (setup as in Simulation 5) for T_d as in (31) and singular values $[\sigma_1 \ \sigma_2] = [2 \ 2]$ of exploration matrix W. The trajectories x_k (_), the first and last m steps (_), the initial state x_0 (•), and the optimizer x^* (•) are depicted.

step-by-step construction of W in [23] one can compute a sequence with nonlinear programming by solving the constrained optimization problem

min
$$\|\operatorname{vec}(W)\|_p^2$$

s.t. $T(W) = T_d$
 $W\mathbb{1} = 0.$ (46)

Instead of the p-norm of $W \in \mathbb{R}^{2n \times m}$, one can in principle choose any other objective function, for example a weighted norm, etc. In contrast to our constructive approach, the sequence

length m with $m \ge \operatorname{rk}(T_d) + 1$ has to be specified in (46). An approximation of the lower bound of m can be computed by following Step 4 of the step-by-step construction procedure for the exploration sequence matrix (see [23]) and choosing the singular values, such that m is minimal.

V. CONCLUSION

In this article, we proposed a novel class of derivative-free optimization algorithms. The idea was to approximate the gradient of the objective function by an m-fold composition of maps. These maps are defined by exploration sequences and generating functions. We provided a general framework for the construction of those ingredients. In particular, the construction of exploration sequences is related to nonholonomic state-transition problems and is based on solving a system of quadratic equations, which we encountered by a singular value decomposition (see Theorem 3). The characterization of the generating functions was carried out by solving the functional (14) (see Theorem 4 and Theorem 5). Numerical simulations and a qualitative study of the dynamics of the algorithm were presented and the role of the algorithm parameters on the behavior of the algorithm was discussed. It turned out that the singular values of the exploration sequence matrix play a crucial role. Due to space limitations, we leave an extensive benchmarking study and comparisons with other derivative-free optimization algorithms for follow up work. The tuning of the algorithm parameters—which entails a choice of exploration sequences and generating functions, and balancing exploration and exploitation by proper step size rules or line search methods—requires systematic and intensive testing for suitable classes of objective functions, which is beyond the scope of this article. Eventually, the tuning of the parameters can be approached, for example, by learning exploration sequences based on a training set of relevant objective functions using an hyperparameter optimization approach. Another future research direction is the extension of the proposed algorithm to extremum seeking problems (cf. [16]) for the two-point algorithmic scheme. Finally, designing exploration sequences plays a key role in our algorithms. This corresponds to the problem of finding sequences, such that the first and second iterated summations, i.e., the one- and two-dimensional projected areas, have the values specified on the right hand sides of (22). To the best of our knowledge, a general and algorithmic characterization of solutions to this inverse problem (i.e., given signature values and find corresponding paths) is not known and in our opinion it is an interesting mathematical research question by its own [27].

APPENDIX A PRELIMINARY LEMMAS

Lemma 2: Let $a \in C^2(\mathbb{R}^n; \mathbb{R})$, $b \in C^0(\mathbb{R}^p; \mathbb{R}^n)$, and $h \in \mathbb{R}_{\geq 0}$. Then for any compact convex set $\mathcal{Z} \subseteq \mathbb{R}^n$ and any compact set $\mathcal{Y} \subseteq \mathbb{R}^p$ there exist an $R \in C^0(\mathbb{R}^n \times \mathbb{R}^p \times \mathbb{R}_{\geq 0}; \mathbb{R})$ and an $M \in \mathbb{R}_{> 0}$, such that for all $z, z + hb(y) \in \mathcal{Z}$ and $y \in \mathcal{Y}$ we have

$$a(z + hb(y)) = a(z) + h\frac{\partial a}{\partial z}(z)^{\mathsf{T}}b(y)$$

$$+R(z,y;h^2) (47)$$

with $|R(z, y; h^2)| \le Mh^2$, i.e., $\lim_{h\to 0} R(z, y; h^2) = 0$.

For the proof of Theorem 2 we refer to [23].

Lemma 3: Let Assumption 1 hold true. Moreover, let $\mathcal{X} \subseteq \mathbb{R}^n$, $\mathcal{J} \subseteq \mathbb{R}$ be compact convex sets and $m \in \mathbb{N}_{\geq 1}$. Then there exist a function $R_{m-1} : \mathbb{R}^n \times \mathbb{R} \times \mathbb{R}_{\geq 0} \to \mathbb{R}^n$ and a constant $M_{m-1} \in \mathbb{R}_{>0}$, such that for any iterates x_0, \ldots, x_m of the algorithm (2) with maps in (5), $x_k, x_k + \sqrt{h}s_k(J(x_k)) \in \mathcal{X}$, and $J(x_k), J(x_k + \sqrt{h}s_k(J(x_k))) \in \mathcal{J}$ we have

$$x_{m} = x_{0} + \sqrt{h}(\alpha_{1} + \alpha_{2}) \sum_{i=0}^{m-1} s_{i}(J(x_{0}))$$

$$+ h\alpha_{2} \sum_{i=0}^{m-1} \frac{\partial s_{i}}{\partial J} (J(x_{0})) s_{i}(J(x_{0}))^{\top} \nabla J(x_{0})$$

$$+ h(\alpha_{1} + \alpha_{2})^{2} \sum_{i=0}^{m-1} \sum_{j=0}^{i-1} \frac{\partial s_{i}}{\partial J} (J(x_{0})) s_{j}(J(x_{0}))^{\top} \nabla J(x_{0})$$

$$+R_{m-1}(x_0, J(x_0); h^{3/2})$$

$$+R_{m-1}(x_0, J(x_0); h^{3/2}) \|_{2} < M_{m-1}h^{3/2}$$
i.e.

with $||R_{m-1}(x_0, J(x_0); h^{3/2})||_2 \le M_{m-1}h^{3/2}$, i.e., $R_{m-1}(x_0, J(x_0); h^{3/2}) = \mathcal{O}(h^{3/2})$.

For the proof of Theorem 3 we refer to [23].

The following two lemmas state the sufficient part of Cauchy's interlacing inequalities [28] for real skew-symmetric matrices. Hence, the imaginary part of the eigenvalues of the principal submatrix can be chosen w.r.t. certain inequalities depending on the eigenvalues of the given skew-symmetric matrix.

Lemma 4: Let $C \in \mathbb{R}^{p \times p}$ be a skew-symmetric matrix with eigenvalues $\pm \eta_k i, \eta_k \in \mathbb{R}_{\geq 0}, k = 1, \dots, \lceil p/2 \rceil$ and let $\omega_\ell \in \mathbb{R}_{\geq 0}, \ell = 1, \dots, \lceil p/2 \rceil - 1$, such that the inequality

$$\eta_1 \ge \omega_1 \ge \eta_2 \ge \omega_2 \dots \ge \eta_{\lceil p/2 \rceil - 1}
\ge \omega_{\lceil p/2 \rceil - 1} \ge \eta_{\lceil p/2 \rceil} \ge 0$$
(49)

is satisfied. Then there exists an unitary matrix $\Theta \in \mathbb{R}^{p \times p}$, such that $Q \in \mathbb{R}^{(p-1) \times (p-1)}$ is a principal submatrix of $\Theta^{\top}C\Theta$ with eigenvalues $\pm \omega_{\ell}i$.

For a proof, we refer to [29].

Lemma 5: Let $C \in \mathbb{R}^{p \times p}$ be a skew-symmetric matrix with eigenvalues $\pm \eta_\ell i, \eta_\ell \in \mathbb{R}_{\geq 0}, \ell = 1, \ldots, p$, arranged according to

$$\eta_1 \ge \eta_2 \ge \ldots \ge \eta_{\lceil p/2 \rceil} \ge 0. \tag{50}$$

Then for $\omega_1 \geq \omega_2 \geq \ldots \geq \omega_r$ with $\omega_k \in \mathbb{R}_{>0}$, such that

$$\eta_k \ge \omega_k \ge \eta_{\lceil p/2 \rceil - r + k} \tag{51}$$

there exists an unitary matrix $\Theta \in \mathbb{R}^{p \times p}$, such that $Q \in \mathbb{R}^{(2r) \times (2r)}$ is a principal submatrix of $\Theta^{\top}C\Theta$ with eigenvalues $\pm \omega_{\ell}i$, $\ell = 1, \ldots, r$.

Proof: Applying Theorem $4 \lceil p/2 \rceil - r$ times, yields the result, similar to the proof of [30, Th. 1].

Appendix A Numerical validation of Conjecture 1: Due to the dependency of C(m) on m in (23), the interlacing lemmas, see Theorem 4 and Theorem 5, are not applicable, since the entries of C(m) change with dimension due to $\epsilon(m)$. We verified

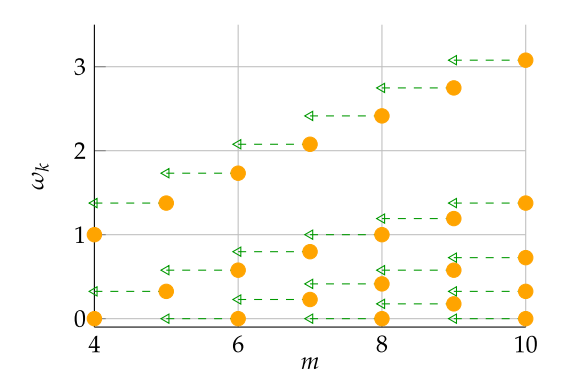


Fig. A1. Illustration of the absolute value of the complex conjugated eigenvalues $\pm \omega_k i$ (•) of \tilde{P} in (27) w.r.t. m for $k=1,\ldots,\lceil m/2\rceil$. The interlacing property (26) is apparent and visualized by the arrows, mapping the eigenvalues to the next lower dimension.

numerically that the interlacing property (26) holds for all $m \leq 10000$. The corresponding Matlab code is available. ¹ Moreover, in Fig. A1 the interlacing property for $4 \leq m \leq 10$ is visualized.

Note that m acts as the exploration sequences' lengths as introduced in (3) and (5), where in the worst case m=4n [cf. (9)]. This implies the property holds for sure for $n \leq 2500$ dimensional problems, which is a very high-dimensional problem for derivative-free algorithms.

Lemma 6: Let W, such that W1=0 be given and set T(W) be as in (12) with $[\alpha_1 \ \alpha_2]=[^1/^2 \ ^1/^2]$. Then the value in the pth row and qth column of T(W) is equivalent to the net area (cf. Gauss area formula in [25]) of the n-sided polygon in the e_p-e_q plane with corner points

$$x_{p,i} = \sum_{k=0}^{i-1} e_p^{\top} w_k, \quad y_{q,i} = \sum_{k=0}^{i-1} e_q^{\top} w_k$$
 (52)

for $i=0,\ldots,m-1$ and $p,q=1,\ldots,2n$, where $x_{p,0}=0$ and $y_{q,0}=0$.

For the proof of Theorem 6 we refer to [23].

APPENDIX B PROOFS

A. Proof Theorem 1

The proof utilizes the result of Theorem 3. Consider the mth step of the evolution of (2) represented by (48) with transition map (5). Let $w_{\ell} = [u_{\ell}^{\top} \ v_{\ell}^{\top}]^{\top}$ for $\ell = 0, \dots, m-1$ and

$$Y(f(z), g(z)) = \begin{bmatrix} f(z)I & g(z)I \end{bmatrix}$$
 (53)

$$\tilde{Y}(f(z), g(z)) = \begin{bmatrix} \frac{\partial f}{\partial z}(z)I & \frac{\partial g}{\partial z}(z)I \end{bmatrix}.$$
 (54)

Then plugging $\{w_\ell\}_{\ell=0}^{m-1}$, $Y(f(J(x_0)),g(J(x_0)))$ and $\tilde{Y}(f(J(x_0)),g(J(x_0)))$ into (48) yields

$$x_m = x_0 + \sqrt{h(\alpha_1 + \alpha_2)}Y(f(J(x_0)), g(J(x_0))) \sum_{i=0}^{m-1} w_i$$

¹[Online]. Available: https://arxiv.org/src/2006.00801v1/anc

$$+ h\tilde{Y}(f(J(x_0)), g(J(x_0))) \left\{ \sum_{i=0}^{m-1} \left(\alpha_2 w_i w_i^\top + (\alpha_1 + \alpha_2)^2 \sum_{j=0}^{i-1} w_i w_j^\top \right) \right\} Y(f(J(x_0)), g(J(x_0)))^\top \nabla J(x_0) + \mathcal{O}(h^{3/2}).$$
(55)

The term in the curly brackets in (55) yields T(W) in (13) and therefore (12) is recovered.

B. Proof Theorem 1

Condition (15) implies

$$w_{m-1} = -\sum_{i=0}^{m-2} w_i. (56)$$

Plugging (56) into (13) yields

$$T(W) = \sum_{i=0}^{m-2} \left(\alpha_2 w_i w_i^{\top} + (\alpha_1 + \alpha_2)^2 \sum_{j=0}^{i-1} w_i w_j^{\top} \right)$$

$$+ \alpha_2 w_{m-1} w_{m-1}^{\top} + (\alpha_1 + \alpha_2)^2 \sum_{i=0}^{m-2} w_{m-1} w_i^{\top}$$

$$= \alpha_2 \sum_{i=0}^{m-2} \left(w_i w_i^{\top} + \sum_{j=0}^{m-2} w_i w_j^{\top} \right)$$

$$+ (\alpha_1 + \alpha_2)^2 \sum_{i=0}^{m-2} \left(\sum_{j=0}^{i-1} w_i w_j^{\top} - \sum_{j=0}^{m-2} w_i w_j^{\top} \right)$$

$$= \alpha_2 \sum_{i=0}^{m-2} \left(w_i w_i^{\top} + \sum_{j=0}^{m-2} w_i w_j^{\top} \right)$$

$$- (\alpha_1 + \alpha_2)^2 \sum_{i=0}^{m-2} \sum_{j=i}^{m-2} w_i w_j^{\top}$$

$$= (\alpha_2 - (\alpha_1 + \alpha_2)^2) \sum_{i=0}^{m-2} \sum_{j=i}^{m-2} w_i w_j^{\top}$$

$$+ \alpha_2 \sum_{i=0}^{m-2} \sum_{j=0}^{i} w_i w_j^{\top} .$$
(58)

Hence, P in (21) is recovered.

C. Proof Theorem 3

Consider (22) and the singular value decomposition of the exploration sequence matrix

$$W = U\Sigma V^{\top} \tag{59}$$

with

$$U = [a_1 \ b_1 \ \cdots a_n \ b_n] \tag{60}$$

$$\Sigma = \begin{bmatrix} \Sigma_0 & 0 \\ 0 & 0 \end{bmatrix}, \ \Sigma_0 = \operatorname{diag}([\sigma_1 \, \cdots \, \sigma_r])$$

$$V = \begin{bmatrix} \Theta - \epsilon \mathbb{1} \, \mathbb{1}^\top \Theta & m^{-1/2} \mathbb{1} \\ -\mathbb{1}^\top \Theta + \epsilon (m-1) \mathbb{1}^\top \Theta & m^{-1/2} \end{bmatrix} \text{ with }$$

$$\epsilon = (m-1)^{-1}(1-m^{-1/2})$$
 and some

$$\Theta \in \mathbb{R}^{(m-1)\times(m-1)} \text{ s.t. } \Theta^{\top}\Theta = \Theta\Theta^{\top} = I.$$
 (62)

Hereby, $a_{\ell} \pm b_{\ell}i$ with $a_{\ell}, b_{\ell} \in \mathbb{R}^{2n}$ for $\ell = 1, \ldots, n$ are the eigenvectors of T_d . Since U, as defined in (60), is constructed by the real and imaginary parts of the eigenvectors of the matrix T_d , U is orthogonal [22]. Moreover

$$X := U^{\top} T_d U = \operatorname{diag}([C_1 \cdots C_n])$$
with $C_{\ell} = \begin{bmatrix} \gamma_{\ell} & -\delta_{\ell} \\ \delta_{\ell} & \gamma_{\ell} \end{bmatrix}, \ \ell = 1, \dots, n$
(63)

where $\gamma_{\ell} \pm \delta_{\ell}i$ are the eigenvalues of T_d with $(2\alpha_2 - (\alpha_1 + \alpha_2)^2)\gamma_{\ell} \in \mathbb{R}_{\geq 0}$ and $\delta_{\ell} \in \mathbb{R}_{\geq 0}$. Note that $\gamma_{\ell} = 0$ and $\delta_{\ell} = 0$ for $\ell > \operatorname{rk}(T_d)$.

The orthogonality of V, given in (62), is shown by direct evaluation

$$V^{\top}V = \begin{bmatrix} \hat{V}_{11} & 0 \\ 0 & 1 \end{bmatrix} \text{ with }$$

$$\hat{V}_{11} = I + (1 - 2\epsilon m + \epsilon^2 m(m-1))\Theta^{\top} \mathbb{1} \mathbb{1}^{\top} \Theta$$

$$(64)$$

$$VV^{\top} = \begin{bmatrix} \tilde{V}_{11} & \tilde{V}_{12} \\ \tilde{V}_{12}^{\top} & \tilde{V}_{22} \end{bmatrix} \quad \text{with}$$

$$\tilde{V}_{11} = I + (\epsilon^2(m-1) + m^{-1} - 2\epsilon) \mathbb{1} \mathbb{1}^\top$$

$$\tilde{V}_{12} = -(\epsilon^2(m-1)^2 - 2\epsilon(m-1) - m^{-1} + 1)1$$

$$\tilde{V}_{22} = \epsilon^2 (m-1)^3 - 2\epsilon (m-1)^2 + m^{-1} + m - 1$$
 (65)

where we used the fact that Θ in (62) is orthogonal. By plugging $\epsilon = (m-1)^{-1}(1-m^{-1/2})$ into (64) and (65), the orthogonality of V, i.e., $VV^\top = V^\top V = I$ is recovered. Now plugging (59) into (22) associated with (63) reveals

$$\begin{bmatrix} \Sigma_0 & 0 \\ 0 & 0 \end{bmatrix} V^{\top} P V \begin{bmatrix} \Sigma_0 & 0 \\ 0 & 0 \end{bmatrix} = X \tag{66}$$

where

$$Q := V^{\top} P V = \begin{bmatrix} \tilde{Q} & * \\ & * \end{bmatrix} \text{ with } \tilde{Q} = \Theta^{\top} \tilde{P} \Theta \text{ and}$$
 (67)

$$\tilde{P} = \left(P - \epsilon (\mathbb{1}\mathbb{1}^\top P + P\mathbb{1}\mathbb{1}^\top) + \epsilon^2 \mathbb{1}\mathbb{1}^\top P\mathbb{1}\mathbb{1}^\top\right)_{1:m-1} \quad (68)$$

with $\tilde{P} \in \mathbb{R}^{(m-1)\times (m-1)}$, which can be written as

$$\tilde{P} = \left(\alpha_2 - \frac{1}{2}(\alpha_1 + \alpha_2)^2\right)$$

$$\times \left[I + (\underbrace{m(m-1)\epsilon^2 - 2m\epsilon + 1}_{=0})\mathbb{1}\mathbb{1}^\top\right]$$

$$+\frac{1}{2}(\alpha_{1}+\alpha_{2})^{2}\begin{bmatrix}0&d_{1}&d_{2}&\dots&d_{m-2}\\-d_{1}&\ddots&\ddots&\ddots&\vdots\\-d_{2}&\ddots&\ddots&\ddots&d_{2}\\\vdots&\ddots&\ddots&\ddots&d_{1}\\-d_{m-2}&\dots&-d_{2}&-d_{1}&0\end{bmatrix}$$
(69)

with $d_i=2i\epsilon-1$ for $i=1,\ldots,m-2$ and ϵ defined in (62), where $\tilde{P}\tilde{P}^\top-\tilde{P}^\top\tilde{P}=0$, hence \tilde{P} normal. More precise, \tilde{P} has complex conjugated eigenvalues $\mu_\ell\pm\omega_\ell i$ with $\ell=1,\ldots,\lceil (m-1)/2\rceil$, where $\mu_\ell=\mu=\alpha_2-1/2(\alpha_1+\alpha_2)^2$ and the skew-symmetric part is a Toeplitz matrix [third line of (69)].

Eventually, (66) imposes the conditions

$$X_{1:r} = \Sigma_0 \tilde{Q}_{1:r} \Sigma_0 \tag{70}$$

$$X_{r+1:n} = 0. (71)$$

with $r = \text{rk}(T_d)$. Then, (71) holds, since there exist n - r - 1 eigenvalues identical to zero and U can be ordered, accordingly. Additionally, let Θ in (62) be of the form, such that

$$\tilde{Q}_{1:r} = \operatorname{diag}([D_1 \cdots D_{\lceil r/2 \rceil}])$$

with
$$D_{\ell} = \begin{bmatrix} \mu & -\hat{\omega}_{\ell} \\ \hat{\omega}_{\ell} & \mu \end{bmatrix}, \ell = 1, \dots, \lceil r/2 \rceil$$
 (72)

holds, where the imaginary part of the eigenvalues of the principal submatrix $\tilde{Q}_{1:r}$ of \tilde{Q} in (67) is denoted by $\pm \hat{\omega}_k i$ for $k=1,\ldots,\lceil r/2\rceil$.

Then (70) implies for $k = 1, \dots, \lceil r/2 \rceil$

$$\mu \sigma_{2k-1}^2 = \mu \sigma_{2k}^2 = \gamma_k$$
 and (73)

$$\sigma_{2k-1}\sigma_{2k}\hat{\omega}_k = \delta_k. \tag{74}$$

In the case of $2\alpha_2 - (\alpha_1 + \alpha_2)^2 = 0$, T_d and \tilde{P} are skew-symmetric due to the assumption in Theorem 3 and (69), respectively. Hence, $\gamma_\ell = 0$ for $\ell = 1, \ldots, n$, and $\mu = 0$, which implies that (73) is satisfied. Equation (74) is satisfied for $k = 1, \ldots, \lceil r/2 \rceil$ with

$$\sigma_{2k} = \delta_k \omega_k^{-1} \sigma_{2k-1}^{-1} \quad \text{and} \quad \sigma_{2k-1} \in \mathbb{R}_{>0}$$
 (75)

where m=r+1 and therefore $\hat{\omega}_k=\omega_k$. Then Θ is constructed as orthogonal transformation similar to U.

In the case $2\alpha_2 - (\alpha_1 + \alpha_2)^2 \neq 0$, (73) and (74) together yield

$$\sigma_{2k-1}^2 = \sigma_{2k}^2 = \frac{\delta_k}{\hat{\omega}_k} = \frac{\gamma_k}{\mu}$$
 (76)

for $k = 1, \ldots, \lceil r/2 \rceil$, hence

$$\hat{\omega}_k = \frac{\delta_k}{\gamma_l} \mu \tag{77}$$

has to be satisfied. Note that δ_k , γ_k , and μ are specified by T_d and α_1, α_2 and $\mu/\gamma_k \geq 0$ due to the positive definiteness condition in Theorem 3. Applying Theorem 5 to \tilde{P} in (67) implies that there exists a Θ , such that (72) and the interlacing property

$$\omega_k \ge \hat{\omega}_k \ge \omega_{\lceil (m-1)/2 \rceil - \lceil r/2 \rceil + k}, \ k = 1, \dots, \lceil r/2 \rceil \tag{78}$$

holds, where $\hat{\omega}_k$ can be chosen in the given intervals. Note that Theorem 5 can be applied to the normal matrix \tilde{P} , due to the decomposition of a scaled unit and skew-symmetric matrix [22]. W.l.o.g., δ_k/γ_k and $\hat{\omega}_k$ are in decreasing order. Then by applying Conjecture 1 (cf. Remark 3) to \tilde{P} in (68) successively, there exists a $m \geq r+1$, such that (78) hold with (77) for all $k=1,\ldots,\lceil r/2\rceil$. \square

D. Proof Theorem 4

Let $2\alpha_2 - (\alpha_1 + \alpha_2)^2 = 0$ and $T(W) = T_d$ is partitioned as in (16). Since T_d has to be skew-symmetric (see also Theorem 3), the eigenvalues of T_d are purely imaginary. Then condition (14) with $T_{12} = -T_{21}^{\top} = -R \in \mathbb{R}^{n \times n}$, where R is arbitrary, reads

$$-I = g'(z)f(z)R^{\top} - f'(z)g(z)R$$

+ $f'(z)f(z)T_{11} + g'(z)g(z)T_{22}.$ (79)

Since, $T_{11} = -T_{11}^{\top}$, $T_{22} = -T_{22}^{\top}$, w.l.o.g. we can express R as $R = I + \tilde{R}$, where $\operatorname{diag}(\tilde{R}) = 0$. Hence, it has to hold

$$g'(z)f(z) - f'(z)g(z) = -1 (80)$$

which is satisfied by the generating functions [31, Th. 1]

$$g(z) = -f(z) \int \frac{1}{f^2(z)} dz.$$
 (81)

Assume that generating functions f and g as in (81) satisfy (80), then condition (79) translates into

$$f'(z)f(z)T_{11} + g'(z)g(z)T_{22} = (f'(z)g(z) + g'(z)f(z))\tilde{R}$$
(82)

implying that $\tilde{R} = -\tilde{R}^{\top}$ holds. Next we consider three cases. Case 1: $\tilde{R} = 0$. Hence

$$f'(z)f(z)T_{11} + g'(z)g(z)T_{22} = 0.$$
 (83)

Clearly, (83) is satisfied by $T_{11} = T_{22} = 0$ with f arbitrary while satisfying g in (81), i.e., (30) results.

For the subcase $a^{-1}T_{11}=b^{-1}T_{22}=:Q$ arbitrary skew-symmetric with $a,b\in\mathbb{R}_{>0},\ f$ and g have to satisfy af'(z)f(z)+bg'(z)g(z)=0, i.e., w.l.o.g. $af^2(z)+bg^2(z)=1$. Accordingly, with (81) and $y'(z)=f^{-2}(z)$ it yields

$$y'(z) = a + by^{2}(z).$$
 (84)

The unique solution of (84) with $\phi \in \mathbb{R}$ is

$$y(z) = \sqrt{\frac{a}{b}} \tan\left(\sqrt{ab}z + \phi\right) \tag{85}$$

and therefore with the definition of y(z) and (81) one reveals (31).

Repeating the above calculations for $a^{-1}T_{11} = -b^{-1}T_{22} =$: Q arbitrary skew-symmetric yields

$$y(z) = \sqrt{\frac{a}{b}} \tanh\left(\sqrt{ab}z + \phi\right) \tag{86}$$

and therefore with the definition of y(z) and (81) one reveals (32).

The remaining subcase $T_{11} \neq \pm aT_{22}$, implies that

$$f'(z)f(z)T_{11} = 0$$
 and $g'(z)g(z)T_{22} = 0$ (87)

since $f'(z)f(z)T_{11}+g'(z)g(z)T_{22}=0$ must hold. If f'(z)f(z)=0 and $T_{11}=Q$ arbitrary skew-symmetric, i.e., $f^2(z)=a$ with $a\in\mathbb{R}_{>0}$, it implies that $f(z)=\sqrt{a}$. Hence, with (81), $g'(z)g(z)\neq 0$ for all $z\in\mathbb{R}$ yields $T_{22}=0$, i.e., (33) results.

The same argumentation holds for g'(z)g(z) = 0 with arbitrary skew-symmetric T_{22} , such that (34) is recovered.

The circumstance that $T_{11} \neq T_{22}$ with $T_{11} \neq 0$ and $T_{22} \neq 0$ is not valid due to (81) and (87). Specifically, f'(z)f(z) = 0 and g'(z)g(z) = 0 has to hold; obviously, based on the above cases, $f(z) = \sqrt{a}$ and $g(z) = \sqrt{a}$ are in conflict with (80).

Case 2: f'(z)g(z) + g'(z)f(z) = 0 for all $z \in \mathbb{R}$. Hence

$$f'(z)f(z)T_{11} + g'(z)g(z)T_{22} = 0$$
 and (88)

$$f'(z)g(z) + g'(z)f(z) = 0 (89)$$

has to be satisfied. Clearly, (88) is satisfied by $T_{11}=T_{22}=0$, where (89) implies -af(z)g(z)=1 with $a\in\mathbb{R}_{>0}$. Accordingly, with (81) and $y'(z)=f^{-2}(z)$ it yields

$$y'(z) = ay(z). (90)$$

The unique solution of (90) with $c \in \mathbb{R}$ is

$$y(z) = e^{az} + c (91)$$

and therefore with the definition of y(z) and (81) one gets (35).

The subcases, where $a^{-1}T_{11} = b^{-1}T_{22} =: Q$ arbitrary skew-symmetric or $T_{11} \neq \pm aT_{22}$ as discussed for Case 1 are not valid. With the same approach as above, i.e., $y'(z) = f^{-2}$ it yields to y'(z) = 0 and therefore no solution for f(z) (and g(z)) can be found or (88) and (89) are not satisfied as discussed in the last paragraph of Case 1, respectively.

Case 3: $\tilde{R} = -\tilde{R}^{\top} \neq 0$. Hence

$$f'(z)f(z)T_{11} + g'(z)g(z)T_{22}$$

$$= (f'(z)g(z) + g'(z)f(z))\tilde{R}.$$
(92)

Clearly, $T_{11} = T_{22} = 0$ is not valid, since $(f'(z)g(z) + g'(z)f(z))\tilde{R} \neq 0$ in this last case.

For the subcase $a^{-1}T_{11} = b^{-1}T_{22} =: Q = -Q^{\top} \neq 0$ with $a,b \in \mathbb{R}_{>0}$, it has to hold that af'(z)f(z) + bg'(z)g(z) = c(f'(z)g(z) + g'(z)f(z)) and $\tilde{R} = cQ$ with $c \in \mathbb{R} \setminus \{0\}$, i.e., w.l.o.g. $a/2f^2(z) + b/2g^2(z) - cf(z)g(z) = 1$. Accordingly, with (81) and $g'(z) = f^{-2}(z)$ it yields

$$y'(z) = \frac{a}{2} + cy(z) + \frac{b}{2}y^{2}(z).$$
 (93)

The unique solution of (93) with $\phi \in \mathbb{R}$ is

$$y(z) = \frac{\sqrt{ab - c^2}}{b} \tan\left(\sqrt{ab - c^2}z + \phi\right)$$
 (94)

and therefore with the definition of y(z) and (81) one reveals (36).

The remaining subcase $T_{11} \neq aT_{22}$, implies that

$$f'(z)f(z)T_{11} - (f'(z)g(z) + g'(z)f(z))\tilde{R} = 0$$
 and

$$g'(z)g(z)T_{22}=0$$
, or (95)
 $g'(z)g(z)T_{22}-(f'(z)g(z)+g'(z)f(z))\tilde{R}=0$ and $f'(z)f(z)T_{11}=0$ (96)

since (92) must hold. However, we show in the sequel that (95) and (96) lead to no new solution or is not valid, respectively.

For (95), $a^{-1}T_{11} = c^{-1}\tilde{R} =: Q = -Q^{\top} \neq 0$ with $a \in \mathbb{R}_{>0}$ and $c \in \mathbb{R} \setminus \{0\}$, it has to hold that af'(z)f(z) = c(f'(z)g(z) + g'(z)f(z)), i.e., w.l.o.g.

$$\frac{a}{2}f^{2}(z) - cf(z)g(z) = 1. (97)$$

Accordingly, with (81) and $y'(z) = f^{-2}(z)$ it yields

$$y'(z) = \frac{a}{2} + cy(z).$$
 (98)

The unique solution of (96) with $d \in \mathbb{R}$ is

$$y(z) = de^{cz} - \frac{a}{2c} \tag{99}$$

and therefore with the definition of y(z) and (81) one gets $f(z)=(cd)^{-1/2} \exp(-c/2z)$ and $g(z)=-(d/c)^{-1/2} \exp(c/2z)$, such that $T_{22}=0$. However, f,g satisfying (97) for all $z\in\mathbb{R}$ only for a=0, hence $T_{11}=0$, i.e, the same result as (35). For (96), $b^{-1}T_{11}=c^{-1}\tilde{R}=:Q=-Q^{\top}\neq 0$ with $a\in\mathbb{R}_{>0}$

For (96), $b^{-1}T_{11} = c^{-1}R =: Q = -Q^{\top} \neq 0$ with $a \in \mathbb{R}_{>0}$ and $c \in \mathbb{R} \setminus \{0\}$, it has to hold that bg'(z)g(z) = c(f'(z)g(z) + g'(z)f(z)), i.e., w.l.o.g.

$$\frac{b}{2}g^{2}(z) - cf(z)g(z) = 1.$$
 (100)

Following the procedure above yields $f(z)=(2)^{-1/2}c^{-1}$ $(b\exp(c/2\,z+d/2)-\exp(-c/2\,z-d/2))$ and $g(z)=2^{1/2}b^{-1}\exp(-c/2z-d/2)$ with $d\in\mathbb{R}$. However, (100) is only satisfied for $d=-cz-\ln(b)$ which leads to f(z)=0 and therefore no valid solution.

Notice that every feasible structure of the skew-symmetric matrix T_d is discussed above case by case, and the differential equations arising in the analysis are solved uniquely. Hence, we believe that the list of triples (T_d,f,g) in Theorem 4 for $2\alpha_2-(\alpha_1+\alpha_2)^2=0$ and T_d skew-symmetric is essentially exhaustive, save for some scaled version of the presented cases. \Box

E. Proof Theorem 5

Let T_d be normal and $(2\alpha_2 - (\alpha_1 + \alpha_2)^2)(T_d + T_d^{\top})$ be positive definite and let $T(W) = T_d$ be partitioned as in (16). Then (14) reads

$$-I = f'(z)f(z)T_{11} + f'(z)g(z)T_{12} + g'(z)f(z)T_{21} + g'(z)g(z)T_{22}.$$
 (101)

Choosing T_d $(T(W) = T_d)$ as in (37), it holds that $(2\alpha_2 - (\alpha_1 + \alpha_2)^2)(T_d + T_d^{\top})$ is positive definite, yielding

$$-1 = a (f'(z)f(z) + g(z)'g(z)) + g'(z)f(z) - f'(z)g(z).$$
 (102)

This equation has been considered in [16]. We refer to the proof of [16, Th. 1] for the derivation of f and g as specified in (37).

Case (38) is analogous to (31). First, note that $(2\alpha_2 - (\alpha_1 + \alpha_2))(T_d + T_d^{\top})$ is positive definite and normal with the given T_d in (38) and $(2\alpha_2 - (\alpha_1 + \alpha_2))(Q + Q^{\top})$ is positive definite and normal, since

$$T_d T_d^{\top} - T_d^{\top} T_d = \begin{bmatrix} Q Q^{\top} - Q^{\top} Q & 0\\ 0 & Q Q^{\top} - Q^{\top} Q \end{bmatrix}$$
 (103)

and

$$T_d + T_d^{\top} = \begin{bmatrix} Q + Q^{\top} & 0\\ 0 & Q + Q^{\top} \end{bmatrix}$$
 (104)

such that the real part of the eigenvalues of Q is identical to that of T_d and therefore the definiteness property is conserved. Hence, the derivation of the generating functions f and g in this case goes along the lines of arguments as used in the proof of Theorem 4 in Appendix B–D, specifically for the case (31), i.e., (84) and (85).

The structure of normal matrices T_d brings more degrees of freedom compared to T_d skew-symmetric as in Theorem 4, and thus, the two cases listed in Theorem 5 are not exhaustive.

REFERENCES

- A. R. Conn, K. Scheinberg, and L. N. Vicente, Introduction to Derivative-Free Optimization. Philadelphia, PA, USA: Siam, 2009.
- [2] Y. Nesterov and V. Spokoiny, "Random gradient-free minimization of convex functions," *Found. Comput. Math.*, vol. 17, no. 2, pp. 527–566, 2017
- [3] J. C. Duchi, M. I. Jordan, M. J. Wainwright, and A. Wibisono, "Optimal rates for zero-order convex optimization: The power of two function evaluations," *IEEE Trans. Inf. Theory*, vol. 61, no. 5, pp. 2788–2806, May 2015.
- [4] V. Torczon, "On the convergence of pattern search algorithms," *SIAM J. Optim.*, vol. 7, no. 1, pp. 1–25, 1997.
- [5] J. C. Spall, "Multivariate stochastic approximation using a simultaneous perturbation gradient approximation," *IEEE Trans. Autom. Control*, vol. 37, no. 3, pp. 332–341, Mar. 1992.
- [6] M. Benosman, Learning-Based Adaptive Control: An Extremum Seeking Approach-Theory and Applications. London, U.K.: Butterworth-Heinemann, 2016.
- [7] S. Wildhagen, S. Michalowsky, J. Feiling, and C. Ebenbauer, "Characterizing the learning dynamics in extremum seeking: The role of gradient averaging and non-convexity," in *Proc. IEEE Conf. Decis. Control*, 2018, pp. 21–26.
- [8] D. Golovin, B. Solnik, S. Moitra, G. Kochanski, J. Karro, and D. Sculley, "Google vizier: A service for black-box optimization," in *Proc. 23rd ACM SIGKDD Int. Conf. Knowl. Discov. Data Mining*, 2017, pp. 1487–1495.
- [9] A. D. Flaxman, A. T. Kalai, and H. B. McMahan, "Online convex optimization in the bandit setting: Gradient descent without a gradient," in *Proc. 16th Annu. ACM-SIAM Symp. Discrete Algorithms*, 2005, pp. 385–394.
- [10] H. Mania, A. Guy, and B. Recht, "Simple random search provides a competitive approach to reinforcement learning," 2018, arXiv:1803.07055.
- [11] J. Feiling, A. Zeller, and C. Ebenbauer, "Derivative-free optimization algorithms based on non-commutative maps," *IEEE Control Syst. Lett.*, vol. 2, no. 4, pp. 743–748, Oct. 2018.
- [12] H.-B. Dürr, M. S. Stanković, C. Ebenbauer, and K. H. Johansson, "Lie bracket approximation of extremum seeking systems," *Automatica*, vol. 49, no. 6, pp. 1538–1552, 2013.
- [13] K. B. Ariyur and M. Krstic, Real-Time Optimization by Extremum-Seeking Control. Hoboken, NJ, USA: Wiley, 2003.
- [14] M. Guay and T. Zhang, "Adaptive extremum seeking control of nonlinear dynamic systems with parametric uncertainties," *Automatica*, vol. 39, no. 7, pp. 1283–1293, 2003.
- [15] Y. Tan, W. Moase, C. Manzie, D. Nešić, and I. Mareels, "Extremum seeking from 1922 to 2010," in Proc. 29th Chin. Control Conf., 2010, pp. 14–26.
- [16] J. Feiling, C. Labar, V. Grushkovskaya, E. Garone, M. Kinnaert, and C. Ebenbauer, "Extremum seeking algorithms based on non-commutative maps," in *Proc. 11th Nonlinear Control Syst.*, 2019, pp. 688–693.

- [17] J. R. Blum, "Multidimensional stochastic approximation methods," *Ann. Math. Statist.*, vol. 25, pp. 737–744, 1954.
- [18] J. Kiefer and J. Wolfowitz, "Stochastic estimation of the maximum of a regression function," Ann. Math. Statist., vol. 23, no. 3, pp. 462–466, 1952.
- [19] H. J. Kushner and D. S. Clark, Stochastic Approximation Methods for Constrained and Unconstrained Systems. Berlin, Germany: Springer, 2012.
- [20] S. Z. Khong, Y. Tan, C. Manzie, and D. Nešić, "Extremum seeking of dynamical systems via gradient descent and stochastic approximation methods," *Automatica*, vol. 56, pp. 44–52, 2015.
- [21] L. Moreau and D. Aeyels, "Practical stability and stabilization," *IEEE Trans. Autom. Control*, vol. 45, no. 8, pp. 1554–1558, Aug. 2000.
- [22] A. Connes, M. R. Douglas, and A. Schwarz, "Noncommutative geometry and matrix theory," *J. High Energy Phys.*, vol. 1998, no. 02, 1998, Art. no. 003.
- [23] J. Feiling, M.-A. Belabbas, and C. Ebenbauer, "Gradient approximation and multi-variable derivative-free optimization based on non-commutative maps," 2020, arXiv:2006.00801.
- [24] C. Altafini, "Nonintegrable discrete-time driftless control systems: Geometric phases beyond the area rule," in *Proc. IEEE 55th Conf. Decis. Control*, 2016, pp. 4692–4697.
- [25] M. Spivak, Calculus on Manifolds: A Modern Approach to Classical Theorems of Advanced Calculus. Boca Raton, FL, USA: CRC Press, 2018.
- [26] A. M. Bloch, "Nonholonomic mechanics," in *Nonholonomic Mechanics and Control*. Berlin, Germany: Springer, 2003, pp. 207–276.
- [27] T. J. Lyons and W. Xu, "Inverting the signature of a path," J. Eur. Math. Soc., vol. 20, no. 7, pp. 1655–1687, 2018.
- [28] A. Cauchy, "Sur l'equation a l'aide de laquelle on détermine les inégalités séculaires des mouvements des planétes," Exer. Math., vol. 9, pp. 174–195, 1891.
- [29] R. Thompson, "Principal minors of complex symmetric and skew matrices," *Linear Algebra Appl.*, vol. 28, pp. 249-255, 1979.
- [30] K. Fan and G. Pall, "Imbedding conditions for Hermitian and normal matrices," Can. J. Math., vol. 9, pp. 298–304, 1957.
- [31] V. Grushkovskaya, A. Zuyev, and C. Ebenbauer, "On a class of generating vector fields for the extremum seeking problem: Lie bracket approximation and stability properties," *Automatica*, vol. 94, pp. 151–160, 2018.



Mohamed-Ali Belabbas received the undergraduate degree in electrical engineering from Ecole Centrale, Paris, France, and Université de Louvain, Ottignies-Louvain-la-Neuve, Belgium, in 2001, and the Ph.D. degree in applied mathematics from Harvard University, Cambridge, MA, USA, in 2007.

He is currently an Associate Professor with the Electrical and Computer Engineering department, the University of Illinois, Urbana-Champaign, Champaign, IL, USA, and with the

Coordinated Science Laboratory. His research interests include networked control system, stochastic control, and geometric control theory.



Christian Ebenbauer received the M.S. degree (Dipl.-Ing.) in telematics (electrical engineering and computer science) from the Graz University of Technology, Graz, Austria, in 2000, and the Ph.D. (Dr.-Ing.) degree in mechanical engineering from the University of Stuttgart, Stuttgart, Germany, in 2005.

He was a Postdoctoral Associate and an Erwin Schrödinger Fellow with the Laboratory for Information and Decision Systems, Massachusetts Institute of Technology, Cambridge,

MA, USA. From April 2009 until July 2021, he was a Full Professor of Computations in Control with the Institute for Systems Theory and Automatic Control, University of Stuttgart. Since August 2021, he has been the head of the Chair of Intelligent Control Systems, RWTH Aachen University, Aachen, Germany. His research interests include dynamical systems, control theory, optimization, and algorithms.



Jan Feiling received the B.Sc. and M.Sc. degrees in engineering cybernetics from the University of Stuttgart, Stuttgart, Germany, in 2014 and 2017, respectively, and the Ph.D. degree in automatic control from the Institute for Systems Theory and Automatic Control, University of Stuttgart, Stuttgart, Germany, in 2021.

During this time, he has served as a Visiting Scholar with the National University of Singapore, Singapore, 2014, and the University of California, Berkeley, CA, USA, from 2016 to

2017. In November 2019, he joined as a full time Professional Venture Architect as the company builder of Porsche Digital GmbH, Forward31, Berlin, Germany. His research interests include optimization, control theory, and machine learning.